

# Sediment fluxes dominate glacial-interglacial changes in ocean carbon inventory: results from factorial simulations over the past 780,000 years

Markus Adloff<sup>1,2</sup>, Aurich Jeltsch-Thömmes<sup>1,2</sup>, Frerk Pöppelmeier<sup>1,2</sup>, Thomas F. Stocker<sup>1,2</sup>, and Fortunat Joos<sup>1,2</sup>

<sup>1</sup>Climate and Environmental Physics, Physics Institute, University of Bern, Switzerland

<sup>2</sup>Oeschger Centre for Climate Change Research, University of Bern, Switzerland

**Correspondence:** Markus Adloff (markus.adloff@unibe.ch)

**Abstract.** Atmospheric CO<sub>2</sub> concentrations varied over ice age cycles due to net exchange fluxes of carbon between land, ocean, marine sediments, lithosphere, and the atmosphere. Marine sediments and polar ice cores archived indirect biogeochemical evidence of these carbon transfers, which resulted from poorly understood responses of the various carbon reservoirs to climate forcing. Modelling studies demonstrated the potential of several physical and biogeochemical processes to impact atmospheric CO<sub>2</sub> under steady-state glacial conditions. Yet, it remains unclear how much these processes affected carbon cycling during transient changes of repeated glacial cycles, and what role burial and release of sedimentary organic and inorganic carbon and nutrients played. Addressing this knowledge gap, we produced a simulation ensemble with various idealized physical and biogeochemical carbon cycle forcings over the repeated glacial inceptions and terminations of the last 780 kyr with the Bern3D Earth system model of intermediate complexity, which includes dynamic marine sediments. The long simulations demonstrate that initiating transient glacial simulations with an interglacial geologic carbon cycle balance causes isotopic drifts that require several 100 kyr to overcome. These model drifts need to be considered when designing spin-up strategies for model experiments. Beyond this, our simulation ensemble allows for gaining a process-based understanding of the transient carbon fluxes resulting from the forcings, and the associated isotopic shifts that could serve as proxy data. We present results of the simulated Earth system dynamics in the non-equilibrium glacial cycles and a comparison with multiple proxy time series. From this we draw several conclusions: In our simulations, the forcings cause sedimentary perturbations that have large effects on marine and atmospheric carbon storage and carbon isotopes. Dissolved Inorganic Carbon (DIC) changes differ by a factor of up to 28 between simulations with and without interactive sediments, while CO<sub>2</sub> changes in the atmosphere are up to four times larger when interactive sediments are simulated. The relationship between simulated DIC (-1800–1400 GtC) and atmospheric CO<sub>2</sub> change (-170–190 GtC) over the last deglaciation is strongly setup-dependent, highlighting the need for considering multiple carbon reservoirs and multi-proxy analyses to more robustly quantify global carbon cycle changes during glacial cycles.

## 1 Introduction

During the Quaternary, the Earth's carbon cycle repeatedly shifted between low atmospheric CO<sub>2</sub> during glacial periods and elevated mixing ratios during interglacials in orbitally-paced cycles (Petit et al., 1999; Siegenthaler et al., 2005; Lüthi et al., 2008). The reconstructed evolution of atmospheric CO<sub>2</sub> from Antarctic ice cores aligns closely with temperature and is lagged by ice sheet extent, suggesting a close coupling of climate and the carbon cycle (e.g. Shackleton, 2000; Bereiter et al., 2015). Yet, simulating atmospheric CO<sub>2</sub> changes that are consistent with reconstructed CO<sub>2</sub> and other proxy data is challenging because the observed carbon cycle changes were the result of complex Earth system responses to climate forcing (Schmittner, 2008).

Changing ocean chemistry is often attributed an important role in these cycles because of the considerable size of the marine carbon reservoir (Broecker, 1982a) and because reconstructions show that overall there was likely less carbon stored on land (in vegetation, permafrost, peatlands and soils) at the Last Glacial Maximum (LGM) than during the current warm period (Yu et al., 2010; Lindgren et al., 2018; Jeltsch-Thömmes et al., 2019). A multitude of physical and biogeochemical processes have been assessed for their contribution to changes in the marine carbon storage on these timescales (e.g. Kohfeld and Ridgwell, 2009; Sigman et al., 2010; Fischer et al., 2010), and their relative importance for the CO<sub>2</sub> difference between the LGM and the late Holocene have been tested in numerical simulations with dynamic ocean models (e.g. Brovkin et al., 2012; Menviel et al., 2012). Changes in ocean circulation and increased CO<sub>2</sub> solubility due to lower temperatures contributed to the lower glacial atmospheric CO<sub>2</sub> concentration (Broecker, 1982a; Smith et al., 1999; Brovkin et al., 2007; Sigman et al., 2010; Fischer et al., 2010), while increased salinity and surface ocean dissolved inorganic carbon (DIC) concentrations due to lowered sea levels tend to counteract this effect by stimulating CO<sub>2</sub> outgassing to the glacial atmosphere (Weiss, 1974; Broecker, 1982a; Brovkin et al., 2007). Furthermore, reduced CO<sub>2</sub> outgassing from the Southern Ocean due to a greater extent of sea ice isolating the surface ocean from the atmosphere, and enhanced stratification due to brine rejection during sea ice formation are other physical processes suggested to have affected the glacial carbon cycle (Stephens and Keeling, 2000; Bouttes et al., 2010).

Marine biogeochemical processes that lead to lower atmospheric CO<sub>2</sub> include a shift of organic carbon remineralization to greater depths, as well as increased export production due to increased nutrient supply to the whole ocean. These processes have opposite effects on export production. Nutrient input from the weathering of emerged shelves (phosphate), changes in nitrogen fixation and denitrification, and enhanced dust deposition (iron, silica) could have boosted export productivity (Broecker, 1982b; Martin, 1990; Pollock, 1997; Deutsch et al., 2004). On the other hand, a reduced return rate of nutrients from the deep ocean into the surface in response to deeper remineralization might have resulted in more efficient nutrient utilization and less export.

In a (hypothetical) closed atmosphere-ocean system, the combination of these processes results in increased marine carbon storage during glacials, but not necessarily in the open Earth system because the carbon removed from the surface ocean and atmosphere by these processes could have been sequestered as particulate carbon in marine sediments in addition to DIC in the water column. Constraints on glacial atmospheric CO<sub>2</sub> can be reconciled with increased and decreased marine DIC inventory in an open system (Jeltsch-Thömmes et al., 2019; Kemppinen et al., 2019), though reproducing reconstructed carbon isotopic changes in atmosphere and ocean seems to require elevated DIC at the LGM (Jeltsch-Thömmes et al., 2019).

It is very probable that changing sedimentary carbonate and particulate organic carbon (POC) burial played a relevant role in glacial-interglacial carbon cycle changes by altering seawater carbonate chemistry, carbonate ion concentrations, carbon isotope ratios, and oxygenation. Particularly, continental shelves have emerged from the ocean during glacial sea level low stands and provided new reef habitats and carbonate deposition environments during deglaciations and interglacials (e.g. Broecker, 1982b; Opdyke and Walker, 1992; Ridgwell et al., 2003; Brovkin et al., 2007; Menviel and Joos, 2012). Additionally, carbonate burial changes in the open ocean have been considered as amplifiers of marine carbon uptake (e.g. Archer and Maier-Reimer, 1994; Kohfeld and Ridgwell, 2009; Schneider et al., 2013; Roth et al., 2014; Kerr et al., 2017; Kobayashi et al., 2021). Organic carbon burial is also prone to vary in response to changes in the rain rate of POC sinking to the sea floor and altered oxygenation. Previous model simulations showed that interactive sediments including POC burial greatly affect atmospheric CO<sub>2</sub> and carbon isotope variations through the burial-nutrient feedback, whereby enhanced burial of organic-bound carbon and nutrients reduces export production (Tschumi et al., 2011; Roth et al., 2014; Jeltsch-Thömmes et al., 2019; Jeltsch-Thömmes and Joos, 2023). Reconstructions of marine burial changes over the last glacial cycle suggest a reduction in globally-integrated inorganic carbon burial (Cartapanis et al., 2018; Wood et al., 2023) during the last glacial period, but increased organic (Cartapanis et al., 2016) sedimentary carbon burial. The magnitudes of both changes are uncertain due to the spatial heterogeneity of sedimentary burial and the inherently local nature of marine archives, but possibly of comparable magnitude to terrestrial carbon stock changes (Cartapanis et al., 2016, 2018). These findings demonstrate that organic and inorganic sedimentary changes and imbalances with weathering fluxes need to be considered when quantifying carbon reservoir changes of the ocean, atmosphere, and land and interpreting the reconstructed changes in CO<sub>2</sub>, carbonate ion concentrations, isotopes, and nutrients over glacial cycles.

Model-based estimates of carbon and carbon isotope inventory differences between glacial and interglacial periods are complicated by temporal carbon cycle imbalances during the continuously evolving climate of glacial cycles. This is particularly challenging when simulating dynamic elemental cycling in and burial from reactive marine sediments and the input of elements by weathering and volcanic outgassing because of long-lasting re-equilibration and memory effects in carbon and nutrient fluxes and particularly isotopic changes (Tschumi et al., 2011; Jeltsch-Thömmes and Joos, 2020). Dynamic sedimentary adjustment, i.e. the equilibration of sedimentary dissolution and remineralization to changes in bottom water which slowly diffuse into sedimentary porewater, and imbalances between the supply (weathering) and loss (sedimentary burial) of carbon and nutrients increase the equilibration time of atmospheric CO<sub>2</sub> by a factor of up to 20 to several tens of thousands of years and the resulting  $\delta^{13}\text{C}$  perturbations take hundreds of thousands of years to recover (Roth et al., 2014; Jeltsch-Thömmes et al., 2019; Jeltsch-Thömmes and Joos, 2023). Importantly, the equilibration time scales are longer than typical interglacials in the late Pleistocene, which opens up the possibility for memory effects that span several glacial cycles.

A caveat of several modeling studies attempting to quantify carbon reservoir sizes at the LGM is that they assume a steady state carbon cycle in a closed (atmosphere-ocean-land, excluding interactive marine sediments) system and do not account for the history of environmental changes that pre-dated the LGM but could have introduced long-lasting memory effects. Transient simulations of an entire glacial cycle with a fully dynamic marine and sedimentary carbon cycle showed that time lags in the carbon cycle response to orbital forcing add constraints for the identification of the processes that caused glacial CO<sub>2</sub>

changes (Menviel et al., 2012). In particular, imbalances between marine carbon burial and continental weathering and the long marine residence time of phosphate delay the CO<sub>2</sub> increase during the temperature rise of deglaciations. Accounting for these long-term effects in the experimental design, transient simulations of more than one glacial cycle showed that reconstructed atmospheric CO<sub>2</sub> and benthic marine δ<sup>13</sup>C changes over the last 400 kyr could be reasonably well simulated with a combination of physical (radiative and ocean volume changes) and biogeochemical processes (carbonate chemistry and land carbon changes, temperature-dependent remineralization depth, additional nutrient supply during glacials, shallow water carbonate burial changes, Ganopolski and Brovkin, 2017). Yet, shallow water carbonate burial was prescribed and POC burial not included in the simulations, which begs the question: what were the effects of the considered processes on glacial-interglacial atmospheric CO<sub>2</sub> and carbon isotopic ratios changes if the sediments are dynamically calculated. Recently, simulations of glacial-interglacial cycles beyond the Mid-Brunhes transition (~430 ka) were run with a box model (Köhler and Munhoven, 2020) and a purely physical model (Stein et al., 2020) which are unable to capture transient and spatially heterogeneous interactive sediments. CLIMBER-2, a fully coupled intermediate-complexity Earth system model, was run stepwise over the last 3 Myr, but the results were not analysed for the carbon cycle dynamics (Willeit et al., 2019).

Here we examine systematically how the transient built-up and dissolution of marine sediments on glacial-interglacial timescales affects the carbon cycle changes produced by the various processes suggested to be relevant on these timescales, a gap left by previous studies. We consider explicitly burial of organic carbon and opal, in addition to CaCO<sub>3</sub>. Instead of searching for the most likely scenario that reconciles the vast proxy evidence, we attempt to gain a more complete process understanding and overview of the proxy-relevant signals that these processes cause in the presence of weathering-burial imbalances. With this goal, we extend factorial simulations of multiple simplified physical and biogeochemical forcings in a marine sediment and isotope-enabled intermediate complexity Earth system model over the last 780 kyr and compare the resulting carbon and carbon isotopic signals to reconstructions. The long timescale is chosen to avoid biases resulting from steady state assumptions and account for the possibility of memory effects under continuously varying climate and carbon cycle that could span multiple glacial cycles. Consequently, all carbon stores are achieved dynamically rather than being prescribed. We present two sets of simulations with and without interactive sediments to distinguish the role of interactive sediments in the carbon cycle changes caused by the tested forcings over reoccurring glacial cycles of the last 780 kyr.

## 2 Methods

### 2.1 Bern3D v2.0s

We simulated the Earth system's transition through the last 780 kyr of glacial cycles with the intermediate complexity Earth system model Bern3D v2.0s, which has an irregular 41×40 grid (lowest resolution: lat×lon = 5°×10° in the North Pacific, highest resolution: lat×lon = 3°×7° in the Equatorial Atlantic) in the horizontal and 32 logarithmically spaced ocean depth layers. The model combines modules for 3D physical ocean dynamics, marine biogeochemistry, marine interactive sediments, and atmospheric energy-moisture balance.

The physical ocean component transports tracers through the ocean by advection, convection, and diffusion. Euphotic zone production depends on temperature, light, sea ice cover, and nutrient (phosphate, iron, silica) availability (Parekh et al., 2008; 125 Tschumi et al., 2011) and explicitly calculates carbon isotope dynamics (Jeltsch-Thömmes et al., 2019). In our setup, a fraction of the particulate organic matter formed in the surface ocean is instantly remineralized following an oxygen concentration dependent version of the globally-uniform Martin curve (Battaglia and Joos, 2018) and particulate inorganic carbon and opal dissolution occurs according to globally-uniform e-folding profiles. The remaining solid particles reaching the sediment-ocean interface enter reactive sediments, where they are preserved, remineralized, or redissolved depending on dynamically calcu- 130 lated porewater chemistry, and mixed by bioturbation (Tschumi et al., 2011).  $\text{CaCO}_3$  dissolution rates in the sediments are determined from the pore water saturation state, and POC remineralisation is parameterised by a linear dependence on porewater  $\text{O}_2$  (Heinze et al., 1999; Tschumi et al., 2011). The model contains 10 layers of reactive sediments. As matter gets pushed downward out of the bottom layer ('sedimentary burial'), it is lost to the modelled inventories. These loss fluxes of C,  $^{13}\text{C}$ , Alk, P, and Si are at equilibrium compensated for by a corresponding solute input flux from land into the coastal surface ocean. The 135 (pre-industrial) land-sea mask and bathymetry are fixed throughout the spin-up and simulations.

## 2.2 Model spin-up with interglacial boundary conditions

We spun up the model with pre-industrial boundary conditions in three stages, sequentially coupling all modules, for computational efficiency. First, we forced the ocean circulation and then the atmosphere-ocean carbon cycle as a closed system with pre-industrial climatic conditions and prescribed  $\text{CO}_2$  for 20 kyr. In the next step, the sediment module is coupled and 140 terrestrial solute supply (phosphate, alkalinity, DIC,  $\text{DI}^{13}\text{C}$  and Si) to the ocean is set to dynamically balance the loss through sedimentary burial for 50 kyr. At the end of this stage, the solute input flux, hereafter named 'weathering input', required to balance sedimentary burial is diagnosed (Table S1) and kept constant for the rest of the spin up procedure and throughout our transient experiments. Until this stage, atmospheric  $\text{CO}_2$  and  $\delta^{13}\text{C}$  were prescribed. The spun up model for the pre-industrial was then run for 2000 years as an open system (freely evolving  $\text{CO}_2$  and  $\delta^{13}\text{C}$ ) with radiative forcing that varied linearly from 145 PI to the slightly different MIS19 conditions, the starting point of our experiments. The total length of the spin-up to this point was 72 kyr. To avoid large drifts in carbon isotopes and alkalinity (Jeltsch-Thömmes and Joos, 2023, explained at the end of section 3.5) in the simulations with the forcings that perturbed the carbon cycle the most (PO4, REMI, LAND, CO2T, BGC, ALL, described in the next section), we ran the fully-interactive model with each respective forcing for two glacial cycles (215 kyr) before starting our experiments. We discuss the relevance of initial conditions and imbalances of the geologic carbon cycle at the end of the manuscript. Model limitations due to constant terrestrial solute supply are discussed in the supplementary material (section SI.5). 150

## 2.3 Experimental design

Data constraints on carbon cycle forcings are too sparse to know exact magnitudes and timings of the forcings that might have varied spatially and temporarily over the last eight glacial cycles. An inverse estimation of the forcings from the resulting proxy 155 signals requires a different simulation ensemble and is beyond the scope of our study. Rather than trying to guess the most

proxy consistent forcing amplitudes and patterns, we designed seven simplified forcings, each with one exemplary magnitude, to simulate the generic effects of processes that have been identified as glacial-interglacial carbon cycle drivers. Except for the orbital changes, which were calculated following Berger (1978); Berger and Loutre (1991) and the reconstructed CO<sub>2</sub>, N<sub>2</sub>O and CH<sub>4</sub> curves (Loulergue et al., 2008; Joos and Spahni, 2008; Bereiter et al., 2015; Etminan et al., 2016), which we used  
160 to calculate the radiative forcing of greenhouse gas changes, the amplitudes of the forcings were set to cause noticeable CO<sub>2</sub> or circulation shifts, informed by previous studies (e.g. Tschumi et al., 2011; Menviel and Joos, 2012; Menviel et al., 2012; Jeltsch-Thömmes et al., 2019; Pöppelmeier et al., 2020). We produced timeseries of these forcings by defining a maximum forcing amplitude for the LGM, a minimum for the Holocene and then modulating this amplitude by reconstructed relative changes in the temporal evolution of either Antarctic ice core  $\delta D$  (Jouzel et al., 2007) or benthic  $\delta^{18}O$  (Lisiecki and Raymo,  
165 2005) for each year (Fig. 1). The choice of the isotope record for calculating the instantaneous forcing depends on whether we expect the forcing to evolve synchronously with temperature like  $\delta D$  or have a time lag similar to  $\delta^{18}O$  (see section SI.5 for a discussion of the limitations). In all simulations, we prescribed the radiative effect of CO<sub>2</sub> in the atmosphere, so that all simulations have the same radiative forcing from greenhouse gases despite differences in simulated CO<sub>2</sub>.

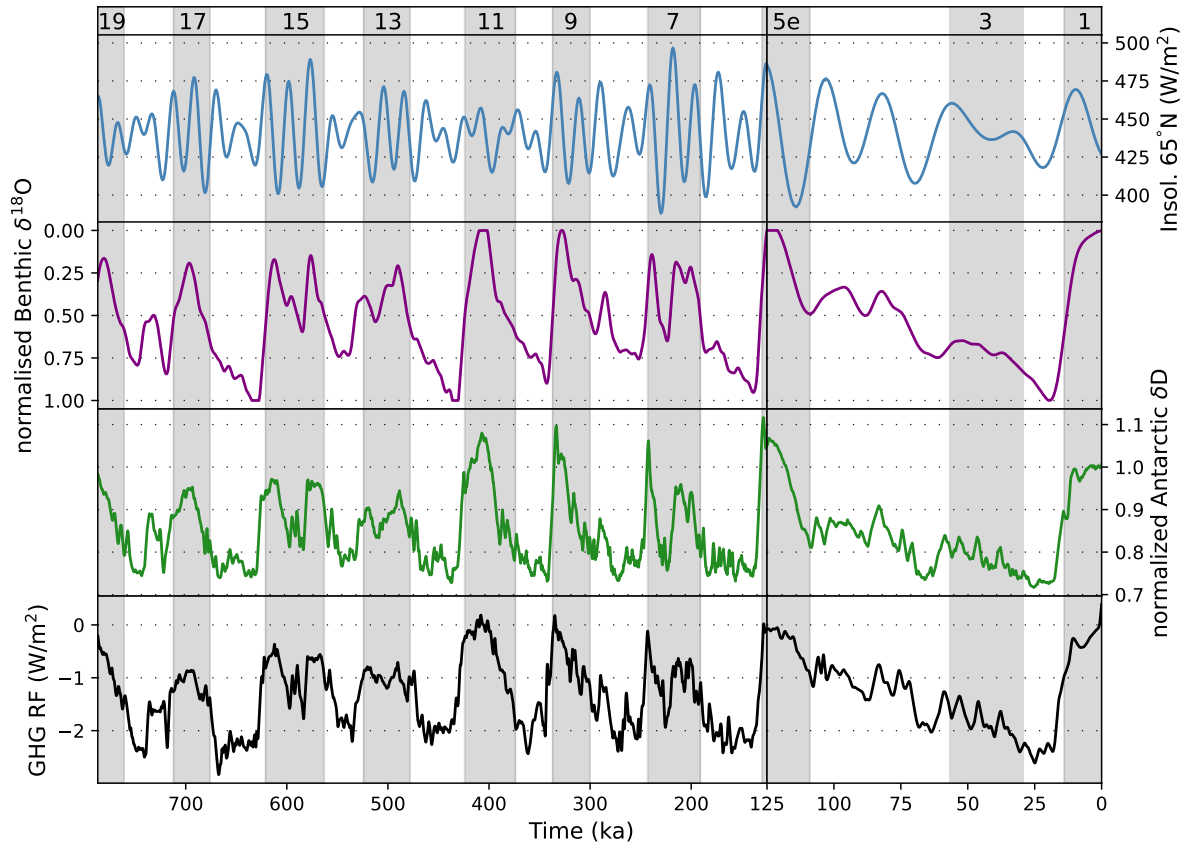


**Figure 1.** Forcing timeseries. Insolation changes (top panel) are calculated according to Berger (1978); Berger and Loutre (1991). The  $\delta^{18}\text{O}$  forcing (second panel) is the LR04 stack (Lisiecki and Raymo, 2005), smoothed by averaging over a 10000-year moving window and normalized to the LGM-PI difference. The  $\delta\text{D}$  forcing (third panel) is taken from Jouzel et al. (2007) and normalized to the LGM-PI difference. The radiative forcing (RF) of  $\text{CO}_2$ ,  $\text{N}_2\text{O}$  and  $\text{CH}_4$  (greenhouse gases 'GHG', bottom panel) is calculated from Bereiter et al. (2015); Loulergue et al. (2008); Joos and Spahni (2008) following Etminan et al. (2016). Gray shading indicate uneven Marine Isotope Stages (MIS).

Specifically, we performed one 'base' run with orbital and radiative forcing only, one model run for different forcings, each  
 170 added to the base forcing, and combinations of the individual forcings to study non-linear effects that appear when processes  
 interact. All of these experiments are run once with and once without interactive sediments, to examine the effect of sediment  
 perturbations on the results. The forcings and their rationale are described below. The experiments are summarized in Table 1.

The application of the standard forcing in simulation BASE causes temperature changes associated with orbital, albedo,  
 and greenhouse gas changes which affect solubility, sea ice and circulation, e.g. slightly weakening AMOC (by up to 4.5 Sv,  
 175 Fig. S8) and resulting in younger deep water masses in the Atlantic and Pacific during the LGM than at the PI, which is  
 inconsistent with proxy data and thus indicates that additional Earth system changes must have occurred (Pöppelmeier et al.,  
 2020). To achieve an older glacial deep ocean (diagnosed with an ideal age tracer), we reduced the wind stress south of  $48^\circ\text{S}$   
 by a maximum of 40% (simulation SOWI) temporally changing proportionately to the  $\delta\text{D}$  change because we assume that

wind strength over the Southern Ocean evolved without temporal lags to Antarctic temperature. As a result, the South Pacific  
180 downwelling is strengthened by up to 1.5 Sv locally in glacials, AMOC strength is further reduced by up to 1 Sv and the  
simulated deep ocean age is  $\sim 100$  years older in the LGM than in the PI, close to published model estimates (Schmittner,  
2003). In this set-up, changing wind stress only affects the circulation, not the piston velocity of gas exchange, which is forced  
by a wind-speed climatology. For an independent assessment of the effect of wind speed changes on sea-air gas exchange, we  
performed a simulation in which we decreased the piston velocity in the Southern Ocean by a maximum of 40 % (KGAS), also  
185 following the evolution of  $\delta D$ . Next, we simulated the additional negative radiative forcing due to increased aerosol loads in the  
glacial atmosphere (AERO, e.g. Claquin et al., 2003) by further reducing the total radiative forcing by a maximum of  $2.5 \text{ W/m}^2$   
during the LGM, modulated by the  $\delta^{18}\text{O}$  record based on the reconstructed correlation between dust and  $\delta^{18}\text{O}$  (Winckler et al.,  
2008, similar to the study of long-term circulation changes in Adloff et al. (2024)). Under this forcing, the AMOC does not  
shut down but weakens by up to 12 Sv relative to PI during glacial maxima due to density changes and sea ice advance in the  
190 North Atlantic (the model behaviour under this forcing is described more extensively in Adloff et al., 2024) and deep North  
Atlantic water mass age rises to up to 1000 years.

In terms of biogeochemical forcings, we mimicked five process that would have occurred during glacial cycles but are not  
dynamically simulated by our model. First, we added a terrestrial carbon sink/source by removing/adding 500 PgC during  
deglaciation/ice age inception to simulate the marine impact of climate-driven carbon cycle changes on land (LAND Jeltsch-  
195 Thömmes et al., 2019). Second, we reduced nutrient limitation on glacial export production (PO4) with a globally-uniform  
addition of phosphate, the only export-limiting nutrient in our model-setup, into the surface ocean, increasing the marine phos-  
phate inventory by 30 % during the glacial maxima. The timeseries of LAND and PO4 are proportional to  $\delta^{18}\text{O}$  changes,  
because we assume that both are lagging behind temperature changes due to continental ice-sheets and changing terrestrial en-  
vironments. Effectively, our nutrient forcing reduces nutrient limitation globally. Rather than simulating the effects of different  
200 nutrient inputs in different regions (e.g. iron in the Southern Ocean, phosphate at shelves), we decided to group all these in one  
simulation with a global forcing because their net effect, increased export production, would be the same in our model, just in  
different regions. This is the only forcing that we did not apply to the model without interactive sediments because, while nu-  
trients can be added to the surface ocean periodically, there is no simple way of artificially extracting nutrients from the ocean  
in return. Third, we reduced the speed of aerobic organic matter remineralization in the ocean to simulate temperature-driven  
205 changes in respiration rates by transitioning between the standard, pre-industrial Bern3D particle profile (Martin scaling) dur-  
ing interglacials and a linear profile in the first 2000 m of the water column (REMI, Fig. S9), following the  $\delta D$  record, since  
we assume that remineralization changes happened synchronously with temperature change. Fourth, we reduced the PIC:POC  
rain ratio by 33 % in the LGM (PIPO) and similarly modulated the forcing timeseries with the  $\delta D$  record. This simulation  
mimics the effect of an ecological shift in marine primary producers on the composition of biogenic marine particles. Fifth, we  
210 performed one run in which we let the model dynamically apply external alkalinity (ALK) fluxes (in addition to the constant  
terrestrial solute supply applied in each simulation, see spin-up methodology) to restore the reconstructed atmospheric  $\text{CO}_2$   
curve (CO2T). In this simulation, the model evaluates the difference between the simulated and reconstructed  $\text{CO}_2$  at each  
time step and adds or removes the marine ALK required to cause the necessary compensatory air-sea carbon flux from the



surface ocean. ALK changes, e.g. due to changes in shallow carbonate deposition or terrestrial weathering, are an effective  
 215 lever for atmospheric CO<sub>2</sub> change (e.g. Brovkin et al., 2007), and this additional run shows the long-term changes in marine  
 biochemistry if this was the dominant driver of glacial-interglacial atmospheric CO<sub>2</sub> change.

**Table 1.** Forcing scenarios. Simulations are run in two configurations: the standard setup with interactive sediments and a closed-system setup without sediments (except PO<sub>4</sub>).

ID	Description	LGM-PI amplitude	Modulating proxy
BASE	orbital changes + radiative effect of greenhouse gasses + ice sheet albedo		CO <sub>2</sub> , CH <sub>4</sub> , δ <sup>18</sup> O
SOWI	BASE + Wind stress strength over Southern Ocean (>48 °S)	-40%	δD
KGAS	BASE + gas transfer velocity in Southern Ocean	-40%	δD
AERO	BASE + Radiative forcing from dust particles	-2.5 W/m <sup>2</sup>	δ <sup>18</sup> O
PHYS	BASE + all physical forcings combined		
LAND	BASE + land carbon storage	-500 PgC	δ <sup>18</sup> O
REMI	BASE + linear glacial remineralization profile in upper 2000m	linear	δD
PIPO	BASE + PIC:POC changes	-0.33	δD
PO <sub>4</sub>	BASE + marine PO <sub>4</sub> reservoir	+30%	δ <sup>18</sup> O
BGC	BASE + all biogeochemical forcings combined		
ALL	BASE + all forcings combined		
CO <sub>2</sub> T	BASE + restoring reconstructed atm. CO <sub>2</sub> concentrations	-90 ppm	CO <sub>2</sub>

For the discussion of the simulations, we quantify the factorial effect of the simulated forcings on different carbon cycle metrics. In simulation BASE, only the standard forcing is active (see table 1), hence the factorial effect of the standard forcing is equal to the simulated change:

$$220 \quad fBASE = BASE$$

In the simulations that combine the standard forcing with one other forcing, the factorial effect of the additional forcing is the difference between the respective simulation and BASE:

$$fFORC = FORC - fBASE$$

In simulations PHYS, BGC and ALL several forcings are combined. We use these simulations to determine non-linearities by  
225 calculating the difference between the results of these simulations and the linear addition of the individual effects of the active  
forcings:

$$nlPHYS = PHYS - (fBASE + fKGAS + fSOWI + fAERO)$$

$$nlBGC = BGC - (fBASE + fREMI + fPO4 + fPIPO + fLAND)$$

$$nlADD = ALL - PHYS - BGC + BASE$$

230  $nlTOT = nlPHY + nlBGC + nlADD$

### 3 Results

The general response of marine biogeochemistry to the applied forcings has been tested and described in previous studies (e.g.  
Tschumi et al., 2008, 2011; Menviel and Joos, 2012; Menviel et al., 2012; Jeltsch-Thömmes et al., 2019; Jeltsch-Thömmes and  
Joos, 2020), here we therefore just provide a brief summary and focus more extensively on their effect on the sediment fluxes.  
235 A more detailed analysis of the model behaviour under each forcing is provided in the supplementary material.

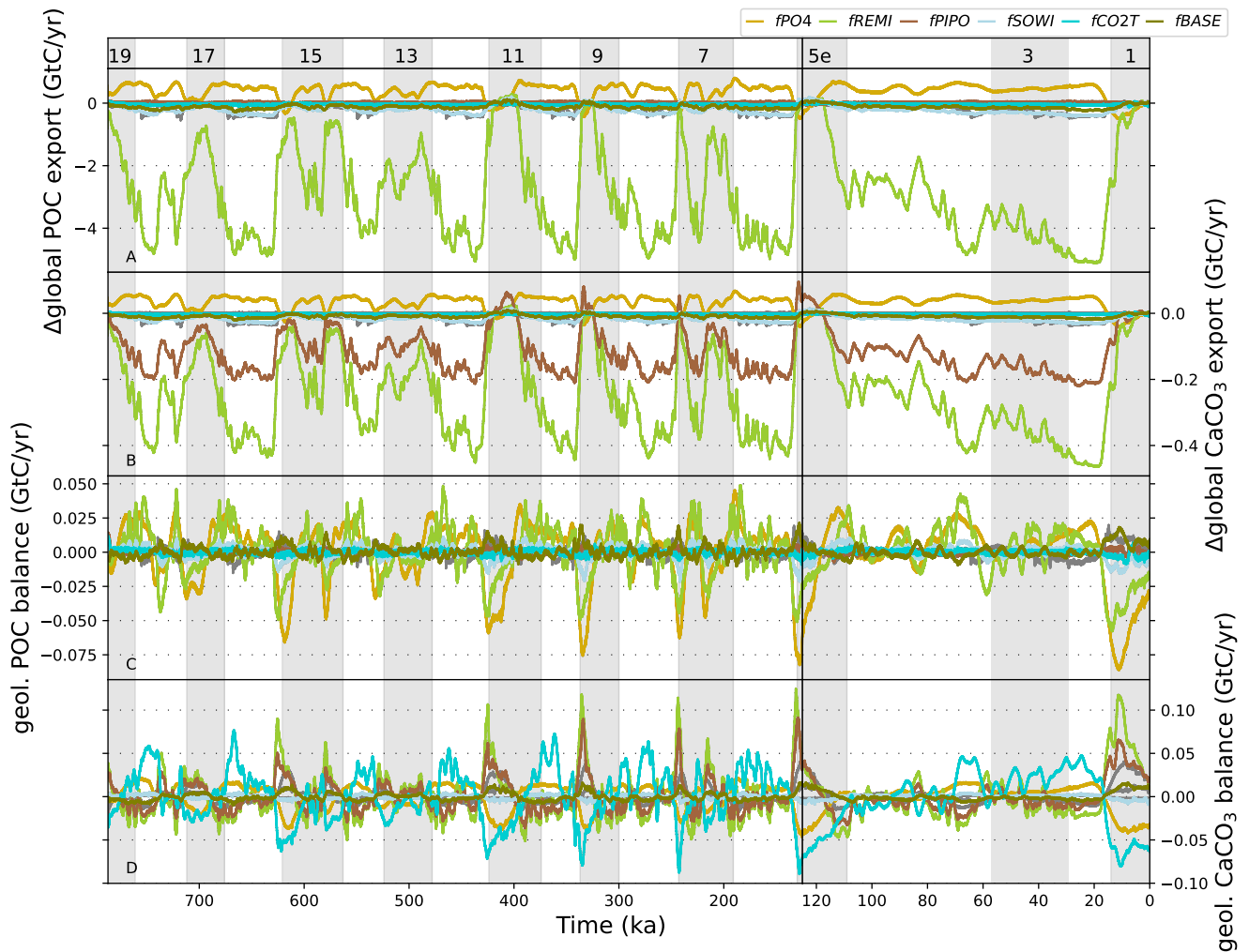


**Figure 2.** Transient changes of POC and  $\text{CaCO}_3$  export production and geologic imbalance (i.e. the difference between accumulation of these materials in marine sediments and the lithosphere minus the constant supply into the surface ocean that mimics terrestrial weathering and volcanism in our simulations) due to the applied forcings. Shown are the factorial differences from pre-industrial for each simulation. The results that are explicitly mentioned in the text are shown in colour, the others are shown in gray. Gray shading indicates uneven MIS as indicated at the top of the figure. See Fig. S10 for absolute rather than factorial differences in each simulations.

In our set-up, carbon exchange between the atmosphere, ocean, and sediments and the burial flux to the lithosphere reacts to climatic and biogeochemical changes while weathering input fluxes of DIC, ALK,  $\text{PO}_4^{3-}$ , Si, and  $^{13}\text{C}$  are constant over time. Thus, a carbon flux imbalance arises in our simulations in response to the applied forcings (Fig. 2 for factorial differences and Fig. S10 for absolute differences). All forcings except  $f_{\text{PO4}}$  reduce global export production during glacial phases (Fig. 2A and B), either due to cooling and expanding sea ice or increased nutrient limitation. In addition to export production, the net exchange of carbon and other elements between sediments and the ocean is changed by the applied forcings via changing

benthic seawater composition, either through circulation, solubility, or biogeochemical changes. Cooling (in *fBASE*) reduces global sediment accumulation rates of  $\text{CaCO}_3$  and POC during glacial phases due to the reduced export production (Fig. 2C and D). In consequence, sequestration of  $\text{CaCO}_3$  and POC from the reactive sediments (i.e. sedimentary burial) is also reduced in response to these forcings, since it is governed by the sedimentary mass accumulation rate. Instead, reduced nutrient limitation during glacial phases (*fPO4*) causes more, rather than less, export production during glacial phases. Deepening of the main remineralization depth (*fREMI*) increases the preservation of sedimentary POC during glacials by reducing marine  $\text{O}_2$ . Hence, under this forcing, POC accumulation is higher during glacial than interglacial phases, while the opposite temporal change occurs for  $\text{CaCO}_3$  accumulation due to reduced  $\text{CaCO}_3$  export production. Increased ALK supply in simulation *CO2T* causes larger sedimentary  $\text{CaCO}_3$  accumulation during glacial phases when ALK input increases  $\text{CaCO}_3$  stability and dissolution events during deglaciations when ALK is removed.

How do the simulated sedimentary changes in our factorial setup compare in magnitude and sign with carbon cycle proxy records?

We discuss this question first by focusing directly on changes in the carbon stored as sedimentary organic and inorganic matter and changes in the benthic carbonate system, before studying their effects on four essential carbon cycle metrics: deep ocean  $\text{CO}_3^{2-}$ , atmospheric  $\text{CO}_2$ , marine DIC, and  $\delta^{13}\text{C}$ . Individual proxy records were selected for their resolution or length. This is not an attempt at a comprehensive compilation of proxy records, nor an attempt to understand individual records in detail. Our simulations are designed to constrain the potential and plausibility of major contributions of the tested forcings to the observed glacial-interglacial atmospheric  $\text{CO}_2$  changes, rather than reproducing a full, realistic scenario. We therefore do not expect that any single simulation presented in our study captures all features of the reconstructed carbon cycle changes over glacial-interglacial cycles. Instead, we investigate in isolation the forcings that would have to some extent occurred simultaneously in reality, and quantify their effects during eight consecutive glacial cycles. Comparing our results to selected proxy records, we discuss processes behind specific patterns of carbon cycle change and the role of weathering-burial imbalances in these.

### 3.1 Sedimentary burial and $\text{CO}_3^{2-}$ concentrations

Reconstructions of global POC burial flux changes over the last glacial cycle (Cartapanis et al., 2016) indicate that POC burial was smallest during interglacials, and gradually rose during glacial phases until it peaked during the LGM. *fSOWI*, *fREMI* and *fPO4* are the only effects which produce higher POC burial fluxes during glacial maxima than during interglacials (Fig. 2), and the latter two are the only ones strong enough to overprint the opposite effect due to cooling (*fBASE*, Fig. S10). However, the simulated increase in POC burial already occurs during the glacial inception, such that the highest burial rates persist throughout most of the glacial phase while in the reconstructions they remain close to the interglacial value through MIS4. Reconstructions of global  $\text{CaCO}_3$  burial changes over the last glacial cycle (Cartapanis et al., 2018) show that burial rates decreased in most ocean basins during glacial inception but increased in the Southern Ocean, resulting in almost no changes in the global average before MIS3. Physical forcings (e.g. *fSOWI* in Fig. 2) do not affect global  $\text{CaCO}_3$  burial rates during glacial inception, consistent with the reconstruction, while *fPO4* and *fCO2T* produce global burial increases and *fPIPO*

and *fREMI* produce decreases between MIS5 and MIS3. However, the physical forcings fail to produce lower  $\text{CaCO}_3$  burial rates during MIS3 and MIS2. *fREMI* and *fPIPO* decrease  $\text{CaCO}_3$  burial during MIS3 and MIS2 but cause much larger burial events in MIS1 than reconstructed (Fig. 2, see also Figs S2, S4, S5, S6, S7).

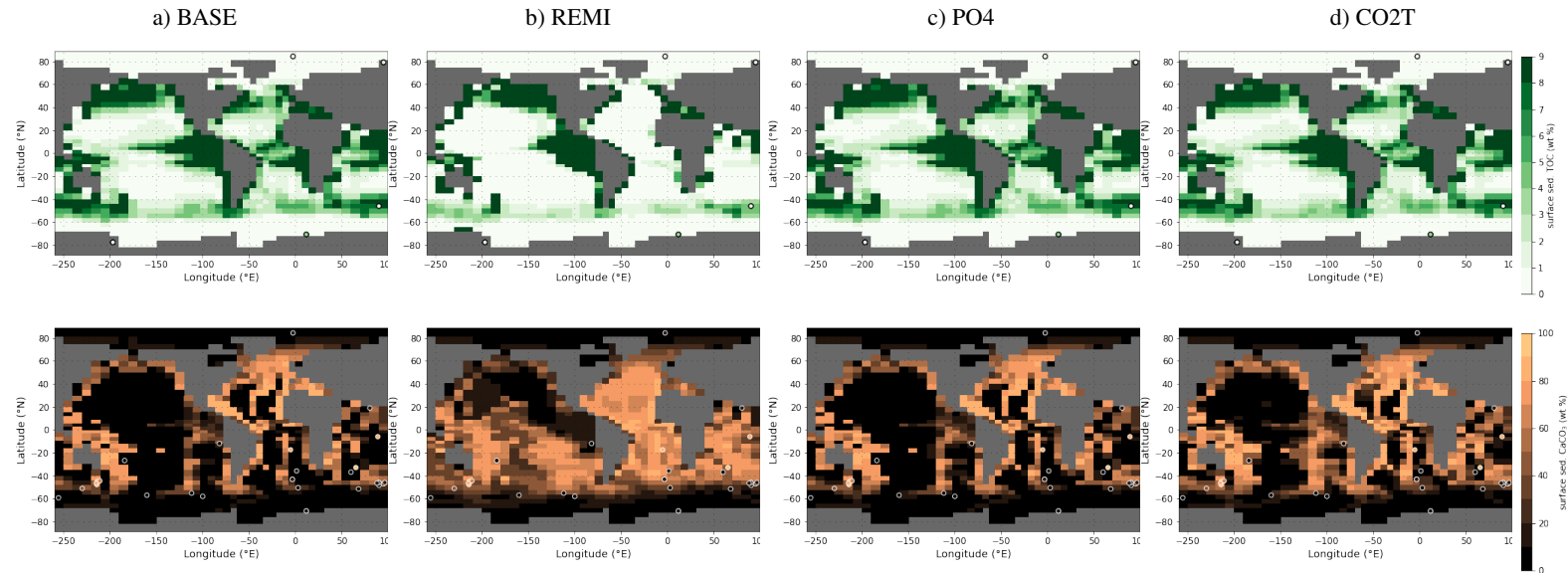


**Figure 3.** Sedimentary POC and  $\text{CaCO}_3$  fractions during LGM as reconstructed (circles, records for POC and  $\text{CaCO}_3$  are from Cartapanis et al., 2016; Wood et al., 2023, , respectively) and in simulations PHYS, REMI, PO4 and CO2T (underlying maps). Shown are only data points that fall into the local benthic grid box of the model. The root mean square errors of simulated and reconstructed values are (from left to right): 7.4 wt %, 3.3 wt %, 7.4 wt % and 6.4 wt % for POC (top row) and 33.6 wt %, 31.5 wt %, 33.3 wt % and 34.4 wt % for  $\text{CaCO}_3$  (bottom row).

Most forcings increase the POC content of surface sediments (top 10 cm) during the LGM (Fig. 3 top row), the exception  
 280 being *fREMI*, which decreases POC outside the East Pacific. However, too few reconstructions exist for depths that are consistent with our model bathymetry for a quantitative model-data comparison. For  $\text{CaCO}_3$ , a few more data points fall within our benthic ocean grid cells. The cooling-related changes (*fBASE*) included in all simulations reproduce a data-consistent carbonate compensation depth (CCD) in most of the Southern Hemisphere extra-tropics but a too high CCD in the tropical South Atlantic and Indian Ocean and a too low CCD off Peru (Fig. 3 bottom row). REMI better captures these tropical CCD  
 285 changes but produces a too low extra-tropical CCD. These model-data differences indicate that different processes might explain the LGM sedimentary composition in different basins, which is not captured by our globally uniform forcings.

The model has been tuned to the pre-industrial  $\text{CaCO}_3$  distribution. However, in our study late Holocene  $\text{CaCO}_3$  contents are the result of almost 800 kyr of transient simulation, which result in imbalances of the geologic carbon cycle at the simulation end even though the forcing is that of the Holocene (Table S2). Differences between the dynamically-achieved and observed  
 290 pre-industrial sedimentary composition add context to the size of the simulated sedimentary fluxes and memory effects. The dynamically-evolved sedimentary POC content is similar across all simulations, while the  $\text{CaCO}_3$  content exhibits large-scale

differences (Fig. S11, S12). Simulations with small sediment perturbations during the glacial cycle (e.g. SOWI, AERO and LAND, Fig. S12) result in  $\text{CaCO}_3$  contents that are similar to Holocene estimates. In simulations REMI and PIPO, the large deglacial  $\text{CaCO}_3$  burial event results in higher sedimentary  $\text{CaCO}_3$  contents in the late Holocene than measured. Simulation 295 CO2T, on the other hand, has less sedimentary  $\text{CaCO}_3$  content during the late Holocene than measured. This is the result of strong dissolution due to forced ALK removal from the open ocean during deglaciations, mimicking e.g. coral reef building. It is therefore less likely that sedimentary  $\text{CaCO}_3$  was perturbed to the extent simulated in REMI, PIPO and CO2T.

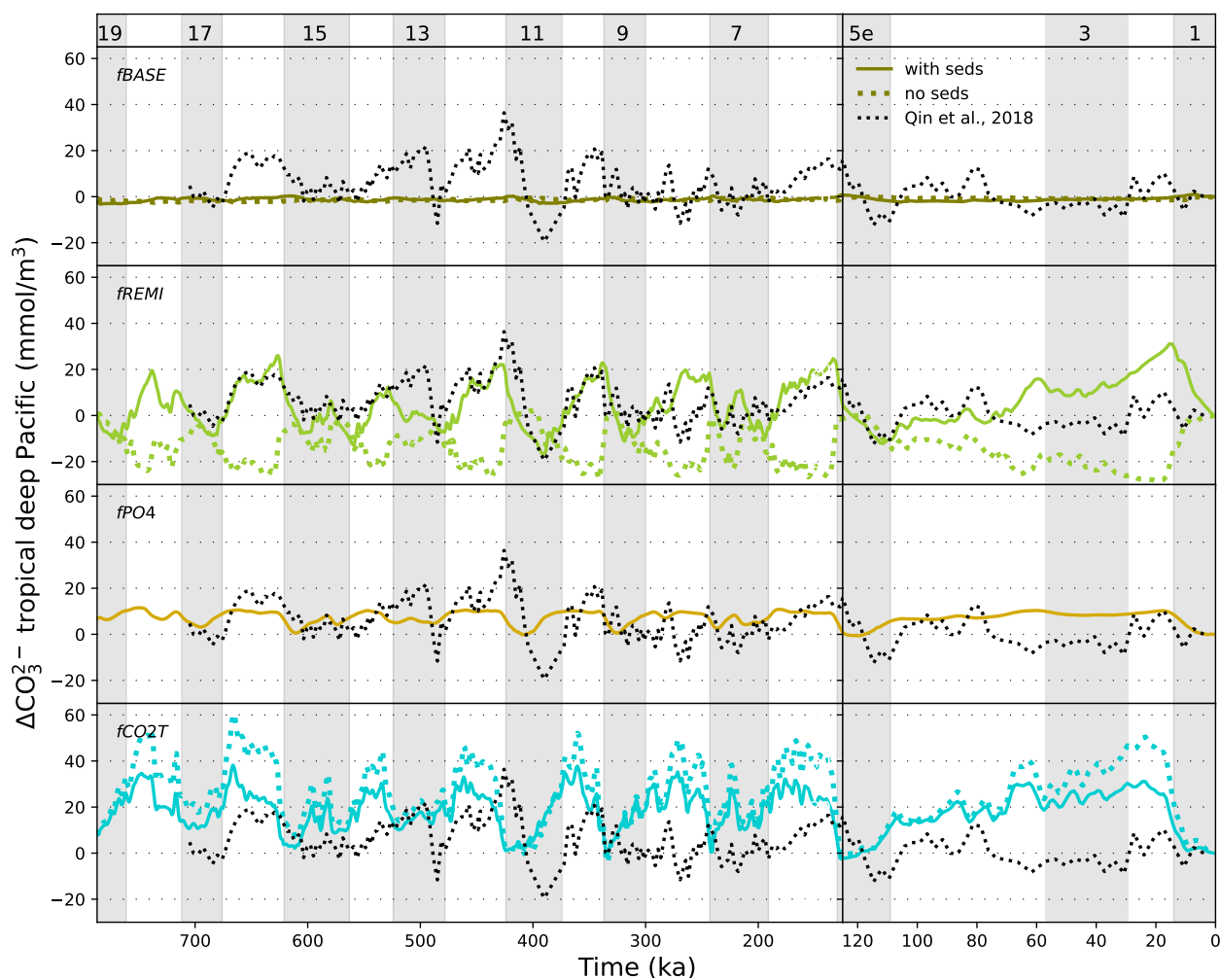


**Figure 4.** Evolution of  $\text{CO}_3^{2-}$  in the tropical deep Pacific as simulated for  $f_{\text{BASE}}$ ,  $f_{\text{REMI}}$ ,  $f_{\text{PO4}}$  and  $f_{\text{CO2T}}$  (from top to bottom) and reconstructed by Qin et al. (2018). The results of the other forcings are shown in Fig. S13.

Next, we address  $[\text{CO}_3^{2-}]$  changes. Kerr et al. (2017) found a repeated pattern of low benthic  $[\text{CO}_3^{2-}]$  in the tropical Pacific and Indian Ocean during interglacials and high  $[\text{CO}_3^{2-}]$  during glacials (difference of 20-55  $\text{mmol/m}^3$ ) throughout the last 500  
300 kyrs. Qin et al. (2018) found that the same pattern extended over the last 700 kyrs, to our knowledge the longest  $[\text{CO}_3^{2-}]$  record. Physical forcings ( $f\text{BASE}$ ,  $f\text{KGAS}$ ,  $f\text{SOWI}$ ,  $f\text{AERO}$ ,  $f\text{PHYS}$ ) and  $f\text{PO4}$  have little effect on deep Pacific  $[\text{CO}_3^{2-}]$  over glacial cycles (Fig. 4, S13). Under the biogeochemical forcings ( $f\text{REMI}$ ,  $f\text{PO4}$ ,  $f\text{PIPO}$ ,  $f\text{LAND}$ ) the simulated glacial-interglacial  $[\text{CO}_3^{2-}]$  difference ranges from a few  $\text{mmol/m}^3$  to 50  $\text{mmol/m}^3$  and is caused by invasion of  $\text{CO}_2$  into the ocean, ALK redistributions within the ocean, and weathering-burial imbalances due to changes of the carbonate export flux  
305 and carbonate compensation (Broecker and Peng, 1987, Fig. 4 and S13).  $f\text{REMI}$  and  $f\text{CO2T}$  cause the largest  $[\text{CO}_3^{2-}]$  changes in the deep equatorial Pacific. For the last glacial cycle, these simulated changes are larger than those reconstructed, suggesting that the forcings cause too large ALK re-distributions within the ocean or carbonate compensation during the last glacial cycle. Interestingly, however, during MIS13-MIS11 and the Mid-Brunhes transition, reconstructed  $[\text{CO}_3^{2-}]$  changes in the deep equatorial Pacific were larger than during the last glacial cycle (Qin et al., 2018, , Fig. 4).  $f\text{CO2T}$  and  $f\text{REMI}$ ,  
310 which produced larger-than-reconstructed  $[\text{CO}_3^{2-}]$  changes over the last glacial cycle, produced  $[\text{CO}_3^{2-}]$  changes more similar to those reconstructed for MIS13-MIS11. The variability of  $[\text{CO}_3^{2-}]$  amplitudes between glacial cycles in the record is not reproduced by any of our forcings.

While the reconstructed deep ocean  $[\text{CO}_3^{2-}]$  reservoir in the Pacific was relatively stable over the last deglaciation, a large  $[\text{CO}_3^{2-}]$  increase was reconstructed for the deep Atlantic (Qin et al., 2018; Yu et al., 2019). The different sensitivities of deep  
315 ocean  $[\text{CO}_3^{2-}]$  in the two basins is also apparent in all of our simulations (see examples in Fig. S14 and S15) and is the result of larger circulation and productivity changes in the Atlantic than Pacific. However, circulation changes produce lower  $[\text{CO}_3^{2-}]$  in the deep sub-polar North Atlantic during the LGM, while reconstructions suggest higher  $[\text{CO}_3^{2-}]$  (Fig. S16A, Yu et al., 2019). Higher deep Atlantic  $[\text{CO}_3^{2-}]$  at the LGM requires increased nutrient supply ( $f\text{PO4}$ ), deeper remineralization ( $f\text{REMI}$ ) or a net ALK input ( $f\text{CO2T}$ ) (Fig. S16B). These patterns appear with and without dynamic sediments in our simulations.  
320 Sediments mostly affect the amplitude and temporal evolution of deep  $[\text{CO}_3^{2-}]$  changes, not their spatial pattern (not shown).

### 3.2 Atmospheric $\text{CO}_2$

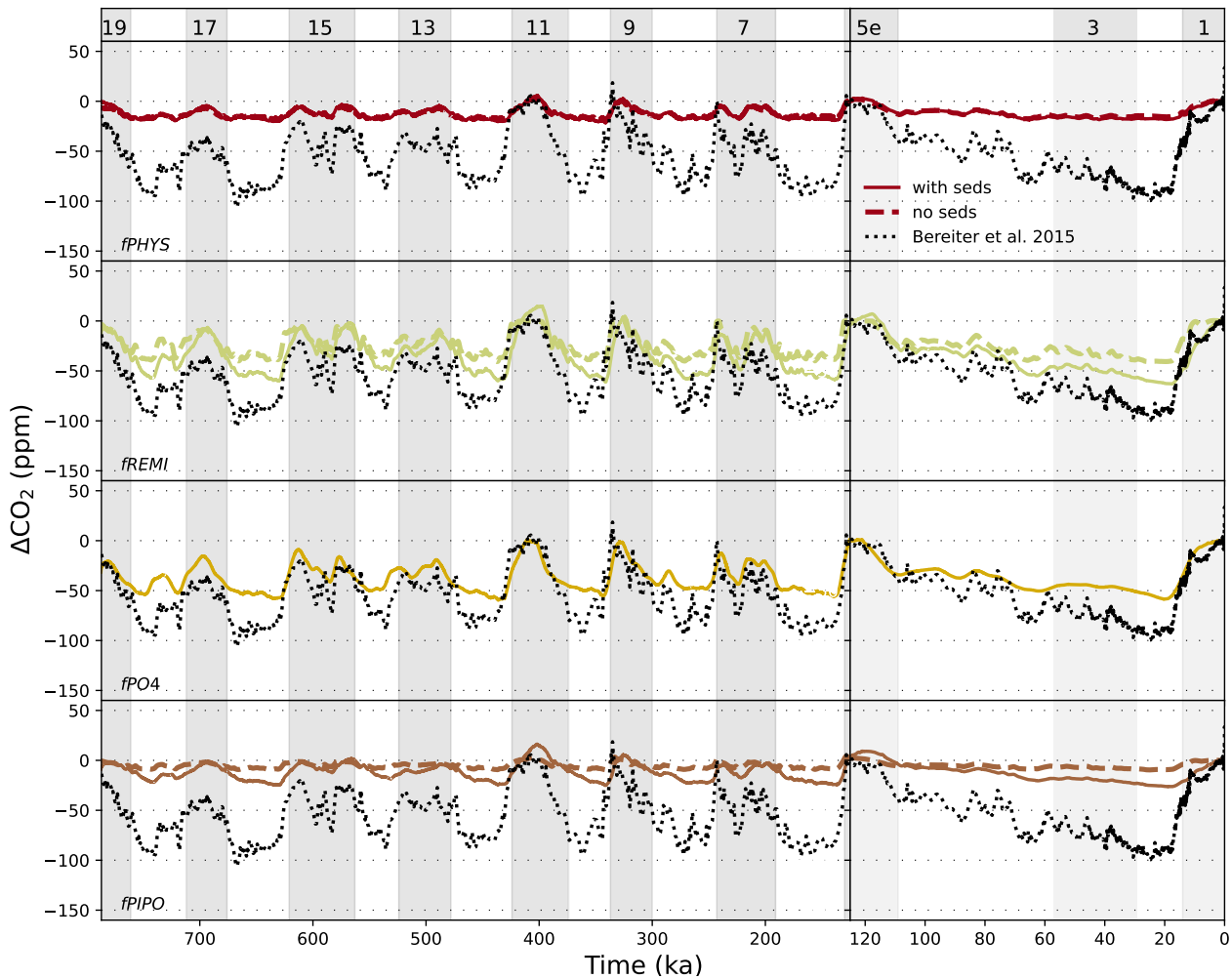


**Figure 5.** Transient variations of atmospheric  $\text{CO}_2$  due to effects  $f_{PHYS}$ ,  $f_{PO4}$ ,  $f_{REMI}$ , and  $f_{PIPO}$  and reconstructed by Bereiter et al. (2015). Shown is the deviation from the pre-industrial value. Gray shading indicates uneven MIS as indicated at the top of the figure. Dashed lines denote runs without sediment module (not available for  $PO4$ ). The same plots for the other simulations are shown in S17.

Interactive sediments have a negligible effect on the atmospheric  $\text{CO}_2$  changes caused by physical forcings but largely alter the  $\text{CO}_2$  change effect of biogeochemical forcings (Fig. 5). Marine  $\text{CO}_2$  uptake and reduced export production due to physical forcings cause a net dissolution/reduced deposition of sedimentary  $\text{CaCO}_3$  during glacials and marine ALK and DIC build up as a consequence. A large fraction of the glacial DIC pool is eventually incorporated into  $\text{CaCO}_3$  and deposited during deglaciations with little effect on outgassing. Under biogeochemical forcings, the larger  $\text{CaCO}_3$  perturbations also have a larger effect on sea-air gas exchange. Another effect is the reduction of sedimentary organic carbon burial rates during interglacials in response to increased nutrient supply ( $f_{PO4}$ ) or a flattened remineralization profile ( $f_{REMI}$ ) during glacial phases. Sedimentary POC accumulates during glacial phases and is subsequently remineralized during deglaciations, raising



330 DIC and reducing ALK, both contributing to enhanced CO<sub>2</sub> outgassing. We explore the forcing-specific differences in more detail by focusing exemplarily on the last deglaciation.

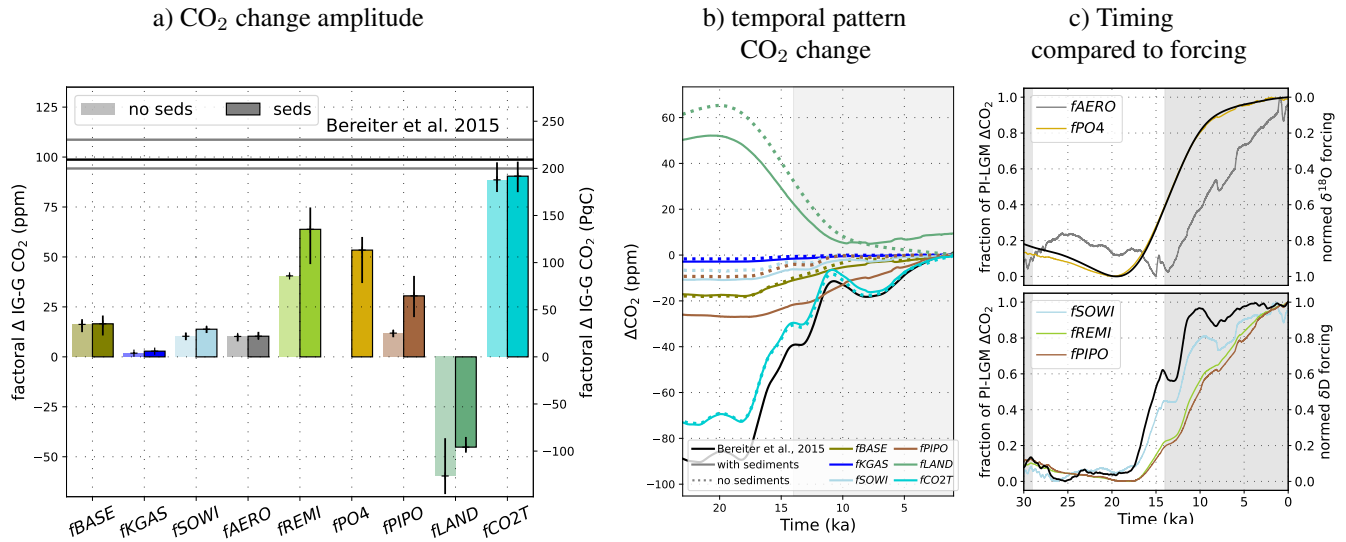


**Figure 6.** Effects of individual forcings on deglacial atmospheric CO<sub>2</sub> changes compared to reconstructions. a) shows the factorial contributions to the mean glacial-interglacial CO<sub>2</sub> amplitude over the last five glacial terminations (excluding terminations before the Mid-Brunhes transition), as well as the range between their minimum and maximum. Light colors indicate results without interactive sediments, full colors indicate results with interactive sediments. The mean, minimum and maximum amplitudes over the last five deglaciations in the ice core record (Bereiter et al., 2015) are shown by the black and gray horizontal lines. b) shows the factors discussed in the text transiently over the last termination. c) shows time lags between the factors and the respective forcing timeseries (black lines). The  $\delta^{18}\text{O}$  and  $\delta\text{D}$  forcings are taken from Lisiecki and Raymo (2005) and Jouzel et al. (2007), respectively (see Methods).

By design, CO<sub>2</sub> restoring causes marine carbon uptake that fills the gap between dynamic atmospheric CO<sub>2</sub> changes of *fBASE* and reconstructions (Fig. 6, S6, S17), so here we focus on the other forcings. Biogeochemical forcings produce the largest CO<sub>2</sub> differences between the LGM and PI with regard to the reconstructions (Fig. 5, 6a). The weathering-burial disequilibrium, which builds up over the glacial phase under these forcings, amplifies the deglacial CO<sub>2</sub> rise, particularly in *fREMI* and *fPIPO*. In both cases, sedimentary accumulation of CaCO<sub>3</sub> spikes during deglaciation, due to increased CaCO<sub>3</sub> export as the forcings wane (Fig. 2). The corresponding ALK reduction expels more CO<sub>2</sub> from the surface ocean into the atmosphere. In the case of *fREMI*, this is further enhanced by a reduction in sedimentary POC accumulation during the deglaciation, which reduces the carbon loss to the sediments. In both cases the sedimentary processes that amplify the deglacial CO<sub>2</sub> rise also reduce its speed and smooth out transient features of the  $\delta\text{D}$  record which are translated into transient atmospheric CO<sub>2</sub> changes in simulations without interactive sediments (Fig 6c). These time lags are caused by the strengthened export production, which counteracts carbon degassing, and a large build-up of ALK and DIC during the glacial phase (amplified by interactive sediments, Fig. S18) which is only gradually reduced by enhanced CaCO<sub>3</sub> burial during deglaciations (Fig. S19). If instead export production and sedimentary carbon accumulation decrease during the deglaciations due to increased nutrient limitation (*fPO4*), the carbon previously incorporated into biogenic matter is outgassed from the surface ocean and no lag between CO<sub>2</sub> rise and the forcing emerges. Weathering-burial imbalances have a smaller effect on circulation-driven deglacial

CO<sub>2</sub> degassing (*fSOWI*, *fAERO*), regarding both amplitude and timing. However, CO<sub>2</sub> also lags temperature in *fAERO* (with and without interactive sediments), due to the hysteresis of the AMOC. Enhanced Southern Ocean wind stress (*fSOWI*) is the only forcing in our simulation set that is able to create fast, transient CO<sub>2</sub> releases despite weathering-burial imbalances.

350 In all simulations except LAND, the lowest CO<sub>2</sub> values occur during the coldest interval of glacial cycles, the glacial maxima (Fig. 5, S17). In all simulations in which the deglacial CO<sub>2</sub> rise lags that of temperature, CO<sub>2</sub> keeps rising throughout the Holocene.

Interactive sediments also affect the sensitivity of the deglacial CO<sub>2</sub> rise to peak interglacial warmth: Only by including interactive sediments does our model simulate a shift in the MBT glacial-interglacial CO<sub>2</sub> amplitude comparable to the observations

355 (Fig. S20, S21).

### 3.3 Marine DIC and the surface carbonate system

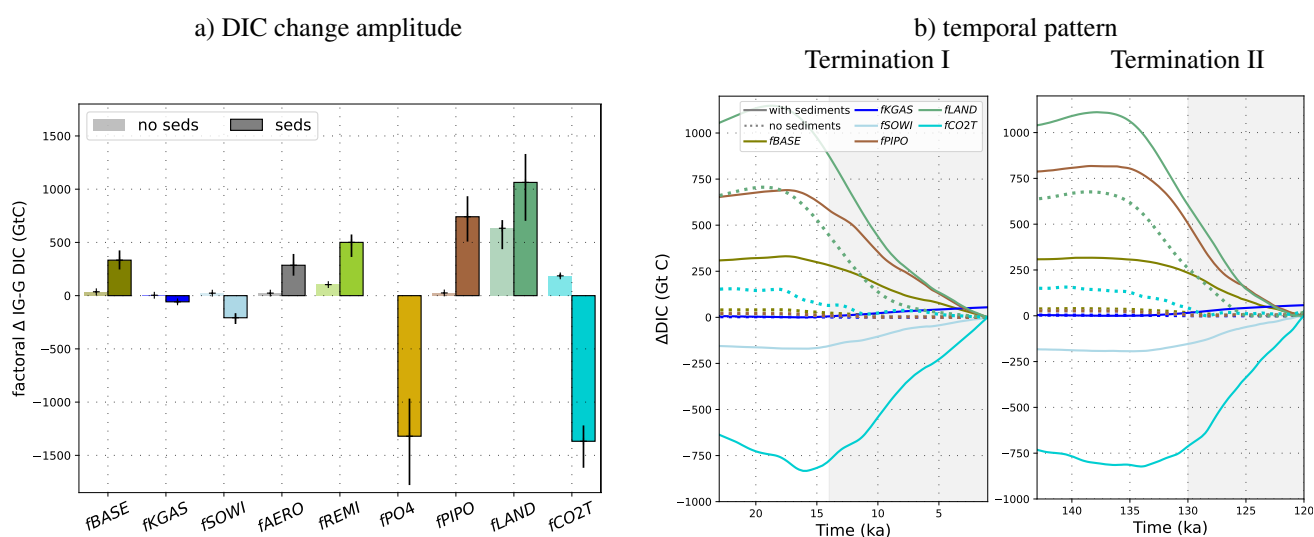


**Figure 7.** Factorial DIC concentration changes for each forcing over glacial cycles, from the highest or lowest DIC value during the glacial cycle, depending on which occurs earlier, to the other extreme. In a) factorial contribution of each forcing to the mean DIC amplitude over the last five glacial cycles, as well as the range between their minimum and maximum. Light colours show the without dynamic sediments, and full colours show the contributions with dynamic sediments. In b) the factorial contribution of selected forcings to the temporal DIC evolutions across two terminations is shown with and without interactive sediments.

Due to interactive sediments in our simulations, increased uptake or release of carbon in the surface ocean does not linearly correlate with DIC changes because marine carbon storage is also affected by changes in the deposition and dissolution fluxes of particulate carbon at the ocean-sediment interface. Interactive sediments affect marine carbon, ALK, and nutrient concentrations in two important ways: Firstly, sediments form a large dynamic reservoir which can store and release large amounts of carbon and nutrients for hundreds to tens of thousands of years. Secondly, sedimentary mass accumulation, dissolution, and remineralization rates control sedimentary burial, the only permanent sink for carbon and nutrients in our simulations

360 and the only mechanism by which environmental change can create imbalances with the prescribed constant solute flux from

land. Fluxes into and out of the sediments respond to environmental change, in some cases on the timescale of water mass  
365 replacement or regional productivity changes. Carbon fluxes from the sediments directly affect the ocean, but not the atmosphere, which causes different amplitudes in the simulated DIC and atmospheric CO<sub>2</sub> changes and different timings of carbon accumulation in ocean and atmosphere. With interactive sediments, *fBASE*, *fAERO*, *fREMI*, *fPIPO* and *fLAND* produce highest DIC during glacial maxima and lowest DIC during interglacials as altered air-sea gas exchange and sediment accumulation result in a net influx of carbon into the ocean during glacial phases. However, while altered air-sea gas exchange  
370 still draws down atmospheric CO<sub>2</sub> under *fKGAS*, *fSOWI* and *fPO4*, larger changes to the sediment fluxes remove carbon from the glacial ocean (Fig. 2) and store excess carbon as carbonate and organic carbon in sediments instead of as DIC in the ocean. Consequently, the lowest DIC occurs during glacial maxima rather than during interglacials under these effects (Fig. S4, S5). *fCO2T* alters sedimentary carbonate preservation such that DIC extremes do not occur at the same time as atmospheric CO<sub>2</sub> extremes, but in between, i.e. the DIC maximum occurs during glaciation and the minimum during deglaciation (Fig. S6).  
375 Furthermore, the onset of the deglacial CO<sub>2</sub> rise in simulations with sediments does not always coincide with the onset of the deglacial DIC change, as is the case in simulations without sediments. This is simulated e.g. for terminations I and II due to *fLAND* and *fCO2T* (Fig. S23), and for terminations I, II, III and IV due to *fPO4* and *fALL* (Fig. S22). Across the tested processes, the corresponding ocean DIC inventory changes from glacial to interglacial are -1800–1400 GtC (Fig. 7) while the atmospheric inventory changes by -170–190 GtC (Fig. 6) over the the same period. For individual processes, DIC changes differ  
380 by a factor of up to 28 between simulations with and without interactive sediments, while CO<sub>2</sub> changes in the atmosphere are maximally four times larger when interactive sediments are considered (Figs 7, 6).

The magnitude of these DIC changes depends on the forcing strength, which varies between glacial cycles. The lukewarm interglacials of the first 350 kyr of our simulations do not restore the export fluxes and sedimentary CaCO<sub>3</sub> preservation required to compensate the prescribed solute influx, and so marine DIC concentrations are persistently higher during 800-450  
385 ka than at PI. Interglacials of the last 450 kyr of the simulation reduce DIC in the long-term because they are warm and long enough for increased carbon transfer into sediments and sediment burial.

### 3.4 $\delta^{13}\text{C}$ in the atmosphere and ocean

$\delta^{13}\text{C}$  in the atmosphere and ocean is also affected by weathering-burial imbalances. Ice cores preserve the  $\delta^{13}\text{C}$  signature of atmospheric CO<sub>2</sub> (Friedli et al., 1984), which showed large fluctuations during the last glacial cycle (Fig. 8), such as  
390 fluctuations of  $\sim 0.5\text{‰}$  during MIS 4 (71-57 ka) and during the last deglaciation ( $\sim 18\text{-}8$  ka) (Eggleston et al., 2016). They also show a long-term increase of atmospheric  $\delta^{13}\text{C}$  across the last glacial cycle (Schneider et al., 2013; Eggleston et al., 2016). Reconstructions of  $\delta^{13}\text{C}$  changes in marine DIC show different trajectories in different ocean basins and water masses (Oliver et al., 2010; Peterson and Lisiecki, 2018). The  $\delta^{13}\text{C}$  signature of marine DIC in a given location and atmospheric CO<sub>2</sub> is influenced by processes which affect the whole marine carbon reservoir (e.g. changes in the amplitude and composition  
395 of marine carbon input or output fluxes), as well as by changes in water mass distribution, export production, and isotopic fractionation during sea-air gas exchange and primary production (Jeltsch-Thömmes et al., 2019; Jeltsch-Thömmes and Joos,

2023), with any signal diluted by the land biosphere. None of the forcings that we applied here produce all of the reconstructed features. However, they show the importance of considering weathering-burial imbalances in their interpretation.

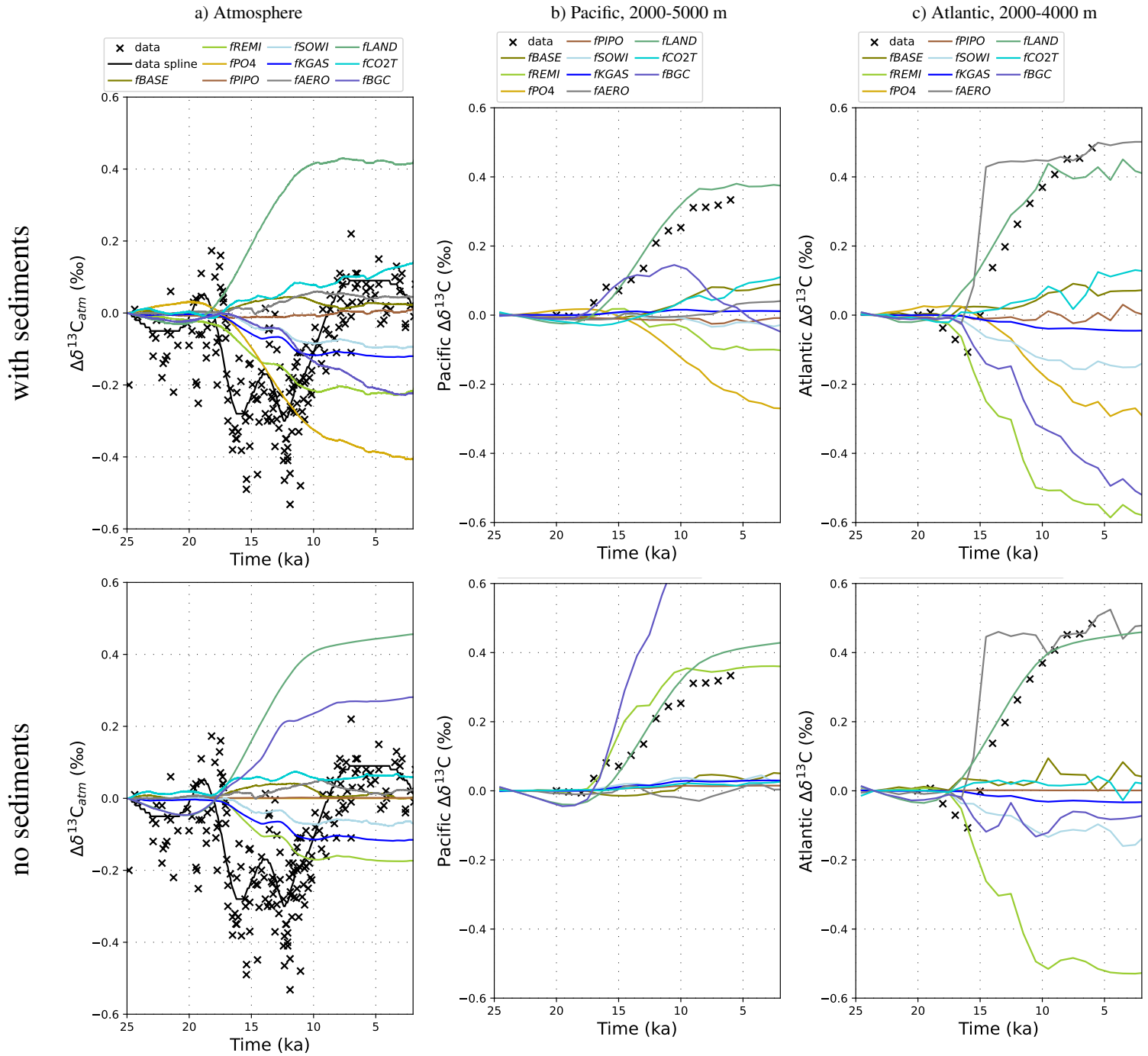


**Figure 8.**  $\delta^{13}\text{C}$  over the last deglaciation in (a) the atmosphere, (b) deep Pacific (120–266°E, -35–55°N) and (c) deep Atlantic (0–65°N) ocean. Lines are simulation results. Crosses are reconstructions from Schmitt et al. (2012), Eggleston et al. (2016) and Peterson and Lisiecki (2018). All results are shown as differences from 24 ka. Results with interactive sediments are shown in the top row and results without sediments are shown in the bottom row.

Fig. 8 shows the factorial effects of the different forcings on atmospheric and marine  $\delta^{13}\text{C}$  across the last deglaciation in comparison to the reconstructed isotopic shifts in these reservoirs. Under *fLAND*,  $\delta^{13}\text{C}$  changes are driven by the simulated release of isotopically light land carbon (-24 ‰) during glacial inceptions and throughout the glacial, resulting in  $\delta^{13}\text{C}$  minima in all reservoirs during glacial maxima and large  $\delta^{13}\text{C}$  increases during deglaciation in response to land carbon uptake, with and without interactive sediments (Fig. 8). This whole ocean shift is the dominant signal in  $\delta^{13}\text{C}$  records of the deep Pacific. In simulations without interactive sediments, *fREMI* also causes a similar shift in the deep Pacific, yet the shift is of opposite sign in simulations with interactive sediments due to the negative geological POC balance during the deglaciation (Fig. 2). *fPO4* has a similar isotopic effect on the ocean as *fREMI* with sediments because it also leads to the release of sedimentary organic carbon during the deglaciation. Since the processes that affect  $\delta^{13}\text{C}_{\text{CO}_2}$  and  $\delta^{13}\text{C}_{\text{DIC}}$  are different, and  $\delta^{13}\text{C}_{\text{DIC}}$  varies between ocean basins, the forcings which best reproduce reconstructed evolution of  $\delta^{13}\text{C}$  also vary between atmosphere and ocean, and specific water masses (Oliver et al., 2010). This indicates that different processes were likely the dominant controls on  $\delta^{13}\text{C}$  regionally, even if they were not necessarily the dominant drivers of atmospheric  $\text{CO}_2$ . The impact of interactive sediments also varies between water masses. For example, in the deep Pacific accumulation of isotopically light  $\delta^{13}\text{C}$  as in *fLAND* likely dominated (Fig. 8b) but must have over-compensated the sediment-enhanced isotopic effects of *fREMI* and *fPO4*, and cannot explain the reconstructed  $\text{CO}_2$  rise (Fig. 6). In the deep North Atlantic, the magnitude of the  $\delta^{13}\text{C}$  shift can also be reproduced by additional radiative cooling and the resulting AMOC shoaling due to *fAERO* (Fig. 8c) and the simulated isotopic shifts are less affected by interactive sediments.

In the atmosphere, the largest  $\delta^{13}\text{C}$  variability (up to  $\pm 0.5$  ‰) is also produced by *fLAND*, with and without interactive sediments, and by *fREMI* and *fPO4* in simulations with interactive sediments. In fact, the gradual trend of reconstructed atmospheric  $\delta^{13}\text{C}$  over the last glacial cycle ( $\sim 0.5$  ‰ from inception to LGM) is only achieved in *fPO4*, the forcing with the biggest effect on sedimentary organic carbon storage (Fig. 2). *fLAND* causes similar long-term changes but of the opposite sign. No simulation captures the large millennial-scale fluctuations in the reconstructions (Fig. 8). Given our smoothed forcing and the absence of freshwater forcings, our simulations do not contain realistic millennial-scale circulation changes, which would likely be required to simulate these fluctuations (Tschumi et al., 2011; Schmitt et al., 2012; Menviel et al., 2015). It is well-established that a complex combination of processes is required to explain the atmospheric  $\delta^{13}\text{C}$  record (e.g. Menviel et al., 2015) but a simulation over the last glacial period or the deglaciation accurately reproducing the reconstructions has not yet been achieved, and reconciling reconstructed with simulated atmospheric  $\delta^{13}\text{C}$  remains a major challenge for future work. However, our simulations show that interactive sediments change the  $\delta^{13}\text{C}$  signals of Earth system changes on deglacial time scales and need to be considered in such future work, despite challenges associated with model spin-up as discussed next.

### 3.5 Long isotopic drifts due to weathering-burial imbalances

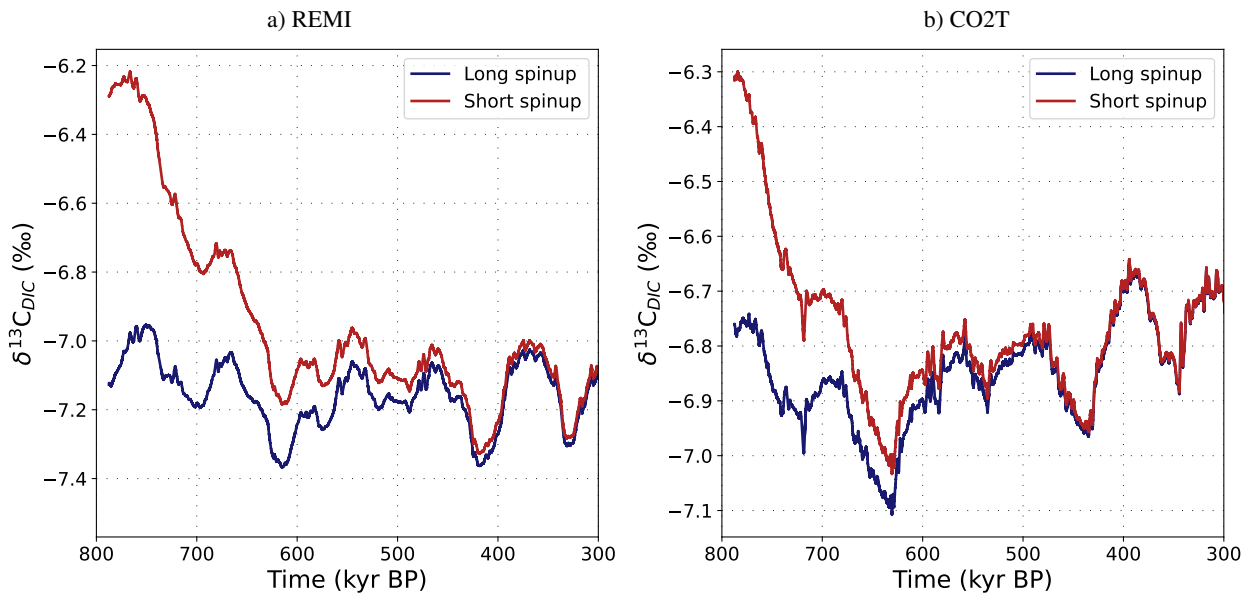


**Figure 9.** Comparison of simulated atmospheric  $\delta^{13}\text{C}$  in simulations REMI and CO2T when started from a 'short spinup', i.e. a 70 kyr PI spinup followed by a 2 kyr adjustment to MIS19 conditions, and a 'long spinup', i.e. the short spinup plus 215 kyr of transiently simulated MIS19-MIS15.

An important technical lesson of our simulations is that the long adjustment timescale in the geologic carbon cycle also presents an initialization problem, especially for carbon isotopes (Jeltsch-Thömmes and Joos, 2023). We started our experiments from MIS19, which was a colder interglacial than the the Holocene, and Holocene conditions were not reached during the lukewarm interglacials of the first 400 kyr of the simulations. In simulations with interactive sediments, the initial imbalance between weathering inputs derived from the pre-industrial spin-up and burial fluxes adjusting to the colder lukewarm interglacials and glacial states caused  $\delta^{13}\text{C}$  drifts during the first glacial cycles (Fig. 9). Consequently, the simulated glacial-interglacial  $\delta^{13}\text{C}$  signal over this period is altered by the long-term adjustment of the geologic carbon cycle. We addressed this issue by transiently simulating two full glacial cycles before starting the experiments. The magnitude of the initial imbalance in the geologic carbon cycle, and hence isotopic drift, depended on the simulated forcing and was largest in simulations REMI, PIPO and CO2T. Importantly, the drift is a result of perturbing the sediment-weathering balance. The drift can therefore not be corrected for with a control simulation without forcing, because it only appears in the perturbed system. Instead, to avoid a drift, the experiment needs to start from an isotopically balanced geologic carbon cycle, which most commonly will require a long spin-up with a fully-coupled, open system, ideally over several glacial cycles especially when simulating large changes of the biological pump or marine carbonate system. We suggest that the size of the transient imbalance of the geologic carbon cycle, and thus the length of the required spin-up, could be minimized by balancing the geologic carbon cycle not for an interglacial state but for the mean burial fluxes over a full glacial cycle.

**Table 2.** Quantified metrics of the carbon cycle according to reconstructions and model responses in our set of simulations with sediments. Shown are the factorial effects of the tested forcings and their non-linearities in comparison with reconstructed differences (LGM minus Holocene) over the last deglaciation (specific times of the comparisons vary slightly by proxy record, depending on temporal resolution and record length, and are indicated in the table header) in various proxy systems. The data references are provided at the bottom of the table. The direction of each arrow indicates whether a difference is positive (pointing upwards, teal-coloured) or negative (pointing downwards, brown-coloured). The width of the arrows shows the size of the difference relative to the reconstruction in the uppermost row "Data". For POM export only qualitative reconstructions exist. Hence, the arrows showing simulated effects are normed by the biggest effect of any forcing.

	$\Delta[\text{CO}_2]$ (ppm)	$\Delta\text{pH}$	$\Delta\text{POM}_{\text{export}}$ (g/m <sup>2</sup> /yr)			$\Delta\delta^{13}\text{C}$ (‰)			$\Delta[\text{CO}_3^{2-}]$ ( $\mu\text{mol/kg}$ )
loc.	global	Eq. Atl.	Iber. Marg.	Eq. Atl.	polar SO	intm. NA	deep NA	deep Pac.	deep Pac.
time	20 - 6 ka	22 - 4 ka	20 - 5 ka			20 - 6 ka			20 - 6 ka
Data									
Factorial Results									
<i>fBASE</i>									
<i>fKGAS</i>		o			o				
<i>fSOWI</i>					o				
<i>fAERO</i>									
<i>fREMI</i>									
<i>fPO4</i>									
<i>fPIPO</i>									
<i>fLAND</i>									
<i>fCO2T</i>									
Non-Linearities									
<i>nlPHYS</i>		o						o	
<i>nlBGC</i>								o	
<i>nlALL</i>									
<i>nlTOT</i>									
Data ref	Bereiter 2015	Hönisch & Hemming 2005	Kohfeld 2005			Peterson 2018			Yu 2013



Table 2 provides an overview of different proxy signals that are produced in by our factorial forcings, and the non-linearities that arise when they are combined, with interactive sediments over the last deglaciation. The first row shows the reconstructed direction of LGM - Holocene differences, and the next lines show the direction and relative size (compared to the proxy signal) of changes induced by the various tested forcings. The last four rows show the direction and relative size of non-linearities caused by three different combinations of the forcings above. For many of the considered proxies, the signals are strongly amplified by the dynamic weathering-burial imbalances, and also the non-linearities are larger with than without interactive sediments. However, the non-linearities are still small compared to the effect of individual biogeochemical forcings, and for some proxies of similar size as the effect of physical forcings. Hence, in most cases, proxy changes provide a first-order constraint on the plausibility of large changes in individual processes. *fBASE*, the effect of temperature changes due to orbital, albedo and greenhouse gas changes, moves almost all proxy systems in the reconstructed direction (the directions of the arrows match), but almost never to the reconstructed extent (the widths of the arrows do not match). It is only sufficient to explain strongly reduced export production in the polar Southern Ocean at the LGM, which in our model is predominantly driven by surface cooling and sea ice expansion regardless of which other processes also occurred.

We identified two processes by which weathering-burial imbalances most effectively raise atmospheric CO<sub>2</sub> during deglaciations in our simulations: ALK removal and organic carbon remineralization. Under *fPIPO* and *fREMI* the combination of high ALK at the end of glacial phases and increased CaCO<sub>3</sub> export production during deglaciation causes large transient CaCO<sub>3</sub> deposition events in the open ocean (Fig. 2) which remove the excess glacial ALK and thus drive a large but slow continuous CO<sub>2</sub> rise compared to the reconstruction. The marine DIC and ALK that built up over the previous glacial phase are too large to be removed instantly, and the resulting large deposition of CaCO<sub>3</sub> during the deglaciation persists far into the interglacial. In consequence, these forcings produce poorer model-data matches for Holocene CaCO<sub>3</sub>. We also showed that the resulting  $\delta^{13}\text{C}$  and [CO<sub>3</sub><sup>2-</sup>] signals in the deep Pacific are not consistent with reconstructions. *fCO2T* shows the effect of forced ALK removal during glaciations to reproduce the reconstructed atmospheric CO<sub>2</sub> record, and can serve to study the effect of ALK removal through means other than deep ocean CaCO<sub>3</sub> burial (e.g. shallow deposition, coral reef growth, reduced terrestrial input) on other proxy systems. This forcing causes deep ocean CaCO<sub>3</sub> dissolution and increasing marine DIC during the deglaciation, moving  $\delta^{13}\text{C}$  in the deep Pacific in the proxy-consistent direction but still producing a large mismatch in [CO<sub>3</sub><sup>2-</sup>]. *fPO4* results in a deglacial CO<sub>2</sub> rise due to a reduction in export production and increased remineralization of sedimentary organic matter which accumulated during the previous glacial period under reduced benthic O<sub>2</sub> concentrations. The resulting CO<sub>2</sub> increase is of similar amplitude as that due to *fREMI* but happens faster, more consistent with the reconstruction. In addition, deep Pacific [CO<sub>3</sub><sup>2-</sup>] is less perturbed by this effect than by *fREMI* or *fCO2T*, yet deep ocean  $\delta^{13}\text{C}$  is shifted in the wrong direction. Future work will have to test which combinations of these processes are most consistent with the wide range of available proxy data.

It is well established that cooling and circulation changes altered sea-air gas exchange and increased deep ocean carbon storage by isolating it from the surface during glacial phases (e.g. Brovkin et al., 2007). Combined, these effects contribute to changes in atmospheric CO<sub>2</sub> in our simulations that are comparable to Brovkin et al. (2012) (26 ppm compared to 30 ppm).

480 Isolating the deep Pacific through reduced Southern Ocean wind forcing (effect *fSOWI*) caused a glacial CO<sub>2</sub> decline by  
~13 ppm, the biggest CO<sub>2</sub> draw-down on top of the effect orbital cooling (*fBASE*) of any isolated physical forcing that we  
tested. Tschumi et al. (2011) showed that this effect also has the potential to cause larger CO<sub>2</sub> draw-down with sedimentary  
amplification than simulated here. The idealised, strong reductions in wind speeds over the Southern Ocean prescribed by  
Tschumi et al. (2011) as a tuning knob for producing old deep ocean waters are unrealistic, but other processes could have  
485 contributed to increased isolation of the deep Pacific. Bouttes et al. (2011) showed that during glacial stages enhanced brine  
rejection during sea ice formation can isolate abyssal waters and cause atmospheric CO<sub>2</sub> and  $\delta^{13}\text{C}$  changes that are similar  
to those reconstructed. Enhanced brine rejection could thus have provided an additional physical process that increased the  
glacial marine carbon storage. The strength of this process, however, is only poorly constrained, and Ganopolski and Brovkin  
(2017) showed that, at a sufficient strength to significantly affect deep ocean carbon storage, this process creates bigger  $\Delta^{14}\text{C}$   
490 anomalies in the deep ocean than reconstructed. Following Menviel et al. (2011), they also argue that the timing of increased  
sea ice formation and atmospheric CO<sub>2</sub> changes during the last deglaciation (Roberts et al., 2016) are not entirely consistent  
with a strong control of brine formation rates on marine carbon storage.

In further agreement with other modelling studies, e.g. Buchanan et al. (2016) and Morée et al. (2021), we find that changing  
the efficiency of the biological pumps (*fREMI*) is an efficient mechanism to achieve glacial-interglacial atmospheric CO<sub>2</sub>  
495 changes similar to those reconstructed from ice cores. However, because of its large effects on deep Pacific  $[\text{CO}_3^{2-}]$  and CaCO<sub>3</sub>  
accumulation during deglaciation it was unlikely the dominant carbon cycle change over the last glacial cycle.

A relevant role of marine sediments, particularly sedimentary CaCO<sub>3</sub>, in glacial-interglacial carbon cycle dynamics has  
long been discussed (e.g. Broecker, 1982b; Broecker and Peng, 1987; Opdyke and Walker, 1992; Archer and Maier-Reimer,  
1994; Raven and Falkowski, 1999) and shown in numerical experiments of differing physical and biogeochemical complexities  
500 (Ridgwell et al., 2003; Joos et al., 2004; Tschumi et al., 2011; Menviel et al., 2012; Roth et al., 2014; Wallmann et al., 2016;  
Ganopolski and Brovkin, 2017; Jeltsch-Thömmes et al., 2019; Köhler and Munhoven, 2020; Stein et al., 2020; Kobayashi  
et al., 2021). In agreement with other studies (e.g. Ganopolski and Brovkin, 2017; Köhler and Munhoven, 2020), we find that  
changing marine ALK can produce large CO<sub>2</sub> changes. Organic carbon storage is less often considered in modelling studies,  
although it also showed significant changes across the last glacial cycle (Cartapanis et al., 2016). Out of the forcings we tested,  
505 reduced nutrient limitation during glacial phases (*fPO4*) produces temporal and regional organic carbon deposition changes  
that were most consistent with the reconstructions. In this simulation, marine sediments turn into a strong carbon sink during  
cold phases. The simulated increased organic carbon deposition during glacial phases reproduces the reconstructed long-term  
trends in atmospheric and surface ocean  $\delta^{13}\text{C}$  during glacials, but is not sufficient in isolation to reproduce the reconstructed  
deep ocean  $\delta^{13}\text{C}$  changes in the Pacific and Atlantic. Thus, while sedimentary organic carbon burial could have provided  
510 a carbon sink during glacial phases, it must have been operating alongside other processes to allow for the reconstructed  
benthic  $\delta^{13}\text{C}$  evolution. Interestingly, processes that increase organic carbon burial during glacial phases (*fPO4*, *fREMI*)  
show that some of the deposited organic carbon can be returned to the ocean during deglaciations with a large potential to  
contribute to a fast post-glacial rise in atmospheric CO<sub>2</sub>. In addition to carbon, nutrients are also removed from the ocean when  
organic matter is buried (Roth et al., 2014). Tschumi et al. (2011) demonstrated in their steady state experiments that increased

515 organic nutrient burial enhances nutrient limitation on export production and reduces  $\text{CaCO}_3$  export, which increases surface  
ALK and amplifies the  $\text{CO}_2$  drawdown caused by the increased burial of organic carbon. Under *fREMI*, this process operates  
transiently. Given the reconstructed increased organic carbon burial rates during glacial maxima, this could have been a relevant  
process over the last glacial cycles, though it might have been reduced in its efficiency by reductions in the PIC:POC of export  
production during glacial phases (Dymond and Lyle, 1985; Sigman and Boyle, 2000). Finally, sedimentary organic carbon  
520 oxidation can also regulate marine ALK by affecting sedimentary  $\text{CaCO}_3$  dissolution (Emerson and Bender, 1981; Sigman  
and Boyle, 2000), but this effect is not directly quantified in our setup. However, we can assess that increased sedimentary  
organic matter remineralization on a global scale during glacial phases does not occur due to any of our tested forcings. On the  
contrary, the effects (*fPO4*, *fREMI*) that increase organic carbon burial during glacial maxima, a prominent feature of the  
reconstructions, decrease globally-averaged sedimentary remineralization rates during glacial times.

525 A close relationship between DIC and  $\Delta^{14}\text{C}(\text{DIC})$  is found in modern deep ocean waters and this relationship has been  
used to reconstruct past DIC changes from radiocarbon reconstructions (Sarnthein et al., 2013). Sedimentary carbon fluxes  
can de-couple deep ocean  $\Delta^{14}\text{C}$  from DIC (Dinauer et al., 2020) and change DIC without altering sea-air carbon transfer,  
meaning that DIC changes do not necessarily imply a comparable  $\text{CO}_2$  change in the atmosphere. In all of our simulations  
with interactive sediments, the DIC inventory change over a glacial cycles is larger than the simultaneous atmospheric  $\text{CO}_2$   
530 inventory perturbation because of changes in carbon reservoirs in sediments and weathering-burial imbalances. Changes in  
the simulated sedimentary burial fluxes result in net transfers of up to 2000 PgC between the carbon pools of the ocean  
and sediments throughout a glacial cycle, while the net loss of atmospheric carbon to reproduce the reconstructed glacial  
 $\text{CO}_2$  is roughly 200 PgC (Sigman and Boyle, 2000; Yu et al., 2010), and the net loss of terrestrial carbon is on the order  
of 500-1000 PgC (Jeltsch-Thömmes et al., 2019). The carbon cycle impact of glacial cycles was thus likely larger in the  
535 ocean than in the atmosphere (Roth et al., 2014; Buchanan et al., 2016), due to changes in sedimentary carbon storage. In  
some of our simulations, large DIC changes are produced by big sustained weathering-burial imbalances during glacials that  
cannot be compensated during the relatively short deglaciations and cause interglacial carbonate preservation patterns that are  
not consistent with observations (Fig. S11, S12). While such simulated scenarios are thus unrealistic, it does not generically  
preclude the possibility of large transient weathering-burial imbalances during glacial phases. Testing a wider range of forcing  
540 magnitudes and combinations with the same model but different set-up, Jeltsch-Thömmes et al. (2019) (the DIC results of  
which are published in the Appendix of Morée et al. (2021)) found a larger DIC change between the pre-industrial and LGM  
than simulated here ( $3900 \pm 550$  GtC compared to a maximum of  $1100 \pm 300$  GtC in Fig. 7) that is consistent with carbonate  
system proxy constraints. Combinations of the tested forcings thus allow for larger transient weathering-burial imbalances than  
produced by our simulation ensemble that can still be reconciled with carbon cycle proxies. Some of the tested forcings also  
545 show lower glacial than inter-glacial DIC (*fPO4*, *fCO2T*) showing that  $\text{CO}_2$  removal from the atmosphere in theory does  
not need to result in increased DIC in the ocean. Instead, these biogeochemical forcings cause sedimentary changes that can  
store large amounts of carbon in inorganic and organic sedimentary matter. Kempainen et al. (2019) and Jeltsch-Thömmes  
et al. (2019) previously showed and discussed the possibility of a negative glacial DIC anomaly due to increased sedimentary  
storage. As found by Jeltsch-Thömmes et al. (2019), organic carbon burial extensive enough to cause a negative glacial DIC

550 anomaly (e.g.  $fPO4$ ) produces large  $\delta^{13}C$  signals of opposite sign than reconstructed, and thus seems unlikely. In the study by  
Jeltsch-Thömmes et al. (2019), a negative glacial DIC anomaly due to ALK-driven  $CaCO_3$  accumulation is also inconsistent  
with the proxy record of the last 25 kyr. Consistently, we find that reconstructed deep Pacific  $[CO_3^{2-}]$  changes make a large-  
scale ALK-driven ( $fCO_2T$ ) glacial  $CaCO_3$  accumulation, which reduces atmospheric  $CO_2$  while also reducing DIC, which  
is unlikely because it causes larger deep Pacific  $[CO_3^{2-}]$  changes than reconstructed over the last deglaciation (Table 2). The  
555 isotopic signal of such large  $CaCO_3$  deposition, however, is smaller than that of POC burial changes and could more likely  
be overprinted by other processes (e.g. terrestrial carbon release and export production changes) to yield proxy-consistent  
evolutions (Table 2).

It has long been suggested that sedimentary imbalances also contributed to the reconstructed interglacial sedimentary  
changes and  $CO_2$  rises after deglaciations (Broecker et al., 1999; Ridgwell et al., 2003; Joos et al., 2004; Broecker and Stocker,  
560 2006; Elsig et al., 2009; Menviel et al., 2012; Brovkin et al., 2016). Consistently we find that  $CO_2$  degassing from the ocean  
persisted throughout deglaciations and into interglacials (e.g. Brovkin et al., 2012), and that the carbon cycle does not reach  
a new equilibrium before the next glacial inception (e.g. supply-burial imbalances in the late Holocene in Table S2). In our  
simulations AMOC hysteresis, sedimentary changes, and delayed temperature responses, e.g. due to ice sheets (mimicked by  
scaling most forcings to the  $\delta^{18}O$  record), introduce memory effects which buffer deglacial carbon cycle reorganizations and  
565 cause continued  $CO_2$  rise throughout interglacials. For example, in PO4, BGC and ALL, the simulations which best align  
with the reconstructed glacial-interglacial organic carbon burial changes, not all glacial organic matter is remineralised and  
carbonate dissolution continued throughout the interglacials.

## 5 Conclusions

In response to different simulated carbon cycle forcings over the repeated glacial-interglacial cycles of the past 780 kyr in the  
570 Bern3D model, we found large sedimentary changes which substantially alter marine carbon and nutrient concentrations and  
spatial distributions. Our simulations show that biogeochemical forcings are required to perturb the sediments sufficiently to  
reproduce reconstructed burial changes and  $CO_3^{2-}$  variations, yet compensating processes (e.g. shallow carbonate deposition)  
must have operated to reduce the buffering impact of this sedimentary perturbation on the deglacial carbon cycle re-organization  
in order to match the speed of the associated carbon release. These results have implications for model experiment design and  
575 the interpretation of  $\delta^{13}C$  proxy data: We showed that the long timescales of ocean-sediment interactions and the weathering-  
burial cycle pose substantial challenges for model spin up because imbalances in the geologic carbon cycle can cause isotopic  
drifts at the beginning of simulations and which are not present in a control run. Depending on the initial isotopic imbalance,  
it takes up to 200 kyr for the drift to subside and the signal of the applied forcing to dominate the simulated transient  $\delta^{13}C$   
changes. Further studies are needed to test whether  $\delta^{13}C$  can be spun up in more computationally-expensive models by com-  
580 bining them with lower-complexity models. In the absence of such a spin up strategy, open system simulations of glacial  $\delta^{13}C$   
are likely strongly affected by these initial drifts severely hampering interpretation of results. These long adjustment timescales  
also pose challenges for separating long-term from short-term signals in the proxy records.

In terms of glacial carbon cycle dynamics, our set of factorial simulations leads to the following conclusions:

585 Firstly, ocean-sediment interactions and related weathering-burial imbalances, including fluxes of nutrients, alkalinity, organic and inorganic carbon, tend to amplify glacial-interglacial CO<sub>2</sub> change.

590 Secondly, the relationship between marine DIC and atmospheric CO<sub>2</sub> changes is not linear across the different forcings and strongly influenced by sediment fluxes. For example, the potential addition of phosphate from exposed continental shelves causes a decrease in atmospheric CO<sub>2</sub> and marine DIC by increasing sedimentary carbon storage. Factorial simulations yield changes in the ocean DIC inventory between -1340 to +1400 GtC and in the atmospheric CO<sub>2</sub> inventory between -96 and 180 GtC (-45 and 80 ppm) over the last five deglaciations in response to individual prescribed physical and biogeochemical forcings. This suggests that approaches utilizing the relationship between radiocarbon and DIC from modern data to reconstruct the ocean's glacial DIC inventory and the postulated corresponding CO<sub>2</sub> change from glacial radiocarbon data may be biased.

595 Thirdly, ocean-sediment interactions strongly impact the evolution of important carbon cycle parameters such as  $\delta^{13}\text{C}(\text{DIC})$  and  $\delta^{13}\text{C}_{\text{CO}_2}$ ,  $\text{CO}_3^{2-}$ , export production, CaCO<sub>3</sub> and POM burial fluxes, preformed and remineralized nutrient concentrations, and oxygen. The interpretation of the proxy records without consideration of weathering-burial imbalances and ocean-sediment interactions for both organic and inorganic carbon may lead to erroneous conclusions.

*Data availability.* All simulation output necessary to produce the figures in this manuscript are available at <https://doi.org/10.5281/zenodo.11385608>

600 *Author contributions.* FP and AJT designed the simulations. AJT ran the simulations. MA processed the model output and drafted the manuscript. MA, AJT, FP, FJ and TFS interpreted the results and edited the manuscript.

*Competing interests.* The authors declare that they have no conflict of interest.

*Acknowledgements.* This research has been supported by the Schweizerischer Nationalfonds zur Förderung der Wissenschaftlichen Forschung (grant nos. 200020-200511 and 200020-200492) and Horizon 2020 (grant nos. 101023443 and 40 820970).

## References

- 605 Adloff, M., Pöppelmeier, F., Jeltsch-Thömmes, A., Stocker, T. F., and Joos, F. (2024). Multiple thermal Atlantic Meridional Overturning Circulation thresholds in the intermediate complexity model Bern3D. *Climate of the Past*, 20(6):1233–1250.
- Archer, D. and Maier-Reimer, E. (1994). Effect of deep-sea sedimentary calcite preservation on atmospheric CO<sub>2</sub> concentration. *Nature*, 367(6460):260–263.
- Battaglia, G. and Joos, F. (2018). Marine N<sub>2</sub>O emissions from nitrification and denitrification constrained by modern observations and  
610 projected in multimillennial global warming simulations. *Global Biogeochemical Cycles*, 32(1):92–121.
- Bereiter, B., Eggleston, S., Schmitt, J., Nehrbass-Ahles, C., Stocker, T. F., Fischer, H., Kipfstuhl, S., and Chappellaz, J. (2015). Revision of the EPICA Dome C CO<sub>2</sub> record from 800 to 600 kyr before present. *Geophysical Research Letters*, 42(2):542–549.
- Berger, A. (1978). Long-term variations of caloric insolation resulting from the Earth's orbital elements. *Quaternary research*, 9(2):139–167.
- Berger, A. and Loutre, M.-F. (1991). Insolation values for the climate of the last 10 million years. *Quaternary science reviews*, 10(4):297–317.
- 615 Börker, J., Hartmann, J., Amann, T., Romero-Mujalli, G., Moosdorf, N., and Jenkins, C. (2020). Chemical weathering of loess and its contribution to global alkalinity fluxes to the coastal zone during the Last Glacial Maximum, Mid-Holocene, and Present. *Geochemistry, Geophysics, Geosystems*, 21(7):e2020GC008922.
- Bouttes, N., Paillard, D., and Roche, D. (2010). Impact of brine-induced stratification on the glacial carbon cycle. *Climate of the Past*, 6(5):575–589.
- 620 Bouttes, N., Paillard, D., Roche, D. M., Brovkin, V., and Bopp, L. (2011). Last Glacial Maximum CO<sub>2</sub> and  $\delta^{13}\text{C}$  successfully reconciled. *Geophysical Research Letters*, 38(2).
- Broecker, W. S. (1982a). Glacial to interglacial changes in ocean chemistry. *Progress in Oceanography*, 11(2):151–197.
- Broecker, W. S. (1982b). Ocean chemistry during glacial time. *Geochimica et cosmochimica acta*, 46(10):1689–1705.
- Broecker, W. S., Clark, E., McCorkle, D. C., Peng, T.-H., Hajdas, I., and Bonani, G. (1999). Evidence for a reduction in the carbonate ion  
625 content of the deep sea during the course of the Holocene. *Paleoceanography*, 14(6):744–752.
- Broecker, W. S. and Peng, T.-H. (1987). The role of CaCO<sub>3</sub> compensation in the glacial to interglacial atmospheric CO<sub>2</sub> change. *Global Biogeochemical Cycles*, 1(1):15–29.
- Broecker, W. S. and Stocker, T. F. (2006). The Holocene CO<sub>2</sub> rise: Anthropogenic or natural? *Eos, Transactions American Geophysical Union*, 87(3):27–27.
- 630 Brovkin, V., Brücher, T., Kleinen, T., Zaehle, S., Joos, F., Roth, R., Spahni, R., Schmitt, J., Fischer, H., Leuenberger, M., et al. (2016). Comparative carbon cycle dynamics of the present and last interglacial. *Quaternary Science Reviews*, 137:15–32.
- Brovkin, V., Ganopolski, A., Archer, D., and Munhoven, G. (2012). Glacial CO<sub>2</sub> cycle as a succession of key physical and biogeochemical processes. *Climate of the Past*, 8(1):251–264.
- Brovkin, V., Ganopolski, A., Archer, D., and Rahmstorf, S. (2007). Lowering of glacial atmospheric CO<sub>2</sub> in response to changes in oceanic  
635 circulation and marine biogeochemistry. *Paleoceanography*, 22(4).
- Buchanan, P. J., Matear, R. J., Lenton, A., Phipps, S. J., Chase, Z., and Etheridge, D. M. (2016). The simulated climate of the Last Glacial Maximum and insights into the global marine carbon cycle. *Climate of the Past*, 12(12):2271–2295.
- Cartapanis, O., Bianchi, D., Jaccard, S. L., and Galbraith, E. D. (2016). Global pulses of organic carbon burial in deep-sea sediments during glacial maxima. *Nature communications*, 7(1):10796.

- 640 Cartapanis, O., Galbraith, E. D., Bianchi, D., and Jaccard, S. L. (2018). Carbon burial in deep-sea sediment and implications for oceanic inventories of carbon and alkalinity over the last glacial cycle. *Climate of the Past*, 14(11):1819–1850.
- Claquin, T., Roelandt, C., Kohfeld, K., Harrison, S., Tegen, I., Prentice, I., Balkanski, Y., Bergametti, G., Hansson, M., Mahowald, N., et al. (2003). Radiative forcing of climate by ice-age atmospheric dust. *Climate Dynamics*, 20(2):193–202.
- Deutsch, C., Sigman, D. M., Thunell, R. C., Meckler, A. N., and Haug, G. H. (2004). Isotopic constraints on glacial/interglacial changes in the oceanic nitrogen budget. *Global Biogeochemical Cycles*, 18(4).
- 645 Dinauer, A., Adolphi, F., and Joos, F. (2020). Mysteriously high  $\Delta^{14}\text{C}$  of the glacial atmosphere: influence of  $^{14}\text{C}$  production and carbon cycle changes. *Climate of the Past*, 16(4):1159–1185.
- Dymond, J. and Lyle, M. (1985). Flux comparisons between sediments and sediment traps in the eastern tropical Pacific: Implications for atmospheric  $\text{CO}_2$  variations during the Pleistocene 1. *Limnology and Oceanography*, 30(4):699–712.
- 650 Edwards, N. R., Willmott, A. J., and Killworth, P. D. (1998). On the role of topography and wind stress on the stability of the thermohaline circulation. *Journal of physical oceanography*, 28(5):756–778.
- Eggleston, S., Schmitt, J., Bereiter, B., Schneider, R., and Fischer, H. (2016). Evolution of the stable carbon isotope composition of atmospheric  $\text{CO}_2$  over the last glacial cycle. *Paleoceanography*, 31(3):434–452.
- Elsig, J., Schmitt, J., Leuenberger, D., Schneider, R., Eyer, M., Leuenberger, M., Joos, F., Fischer, H., and Stocker, T. F. (2009). Stable isotope constraints on Holocene carbon cycle changes from an Antarctic ice core. *Nature*, 461(7263):507–510.
- 655 Emerson, S. and Bender, M. (1981). Carbon fluxes at the sediment-water interface of the deep-sea: calcium carbonate preservation.
- Etminan, M., Myhre, G., Highwood, E. J., and Shine, K. P. (2016). Radiative forcing of carbon dioxide, methane, and nitrous oxide: A significant revision of the methane radiative forcing. *Geophysical Research Letters*, 43(24):12–614.
- Fischer, H., Schmitt, J., Lüthi, D., Stocker, T. F., Tschumi, T., Parekh, P., Joos, F., Köhler, P., Völker, C., Gersonde, R., et al. (2010). The role of Southern Ocean processes in orbital and millennial  $\text{CO}_2$  variations—A synthesis. *Quaternary Science Reviews*, 29(1-2):193–205.
- 660 Friedli, H., Moor, E., Oeschger, H., Siegenthaler, U., and Stauffer, B. (1984).  $^{13}\text{C}/^{12}\text{C}$  ratios in  $\text{CO}_2$  extracted from Antarctic ice. *Geophysical research letters*, 11(11):1145–1148.
- Frings, P. J. (2019). Palaeoweathering: how do weathering rates vary with climate? *Elements: An International Magazine of Mineralogy, Geochemistry, and Petrology*, 15(4):259–265.
- 665 Ganopolski, A. and Brovkin, V. (2017). Simulation of climate, ice sheets and  $\text{CO}_2$  evolution during the last four glacial cycles with an Earth system model of intermediate complexity. *Climate of the Past*, 13(12):1695–1716.
- Griffies, S. M. (1998). The Gent–McWilliams skew flux. *Journal of Physical Oceanography*, 28(5):831–841.
- Hayes, C. T., Costa, K. M., Anderson, R. F., Calvo, E., Chase, Z., Demina, L. L., Dutay, J.-C., German, C. R., Heimbürger-Boavida, L.-E., Jaccard, S. L., et al. (2021). Global ocean sediment composition and burial flux in the deep sea. *Global biogeochemical cycles*, 35(4):e2020GB006769.
- 670 Heinze, C., Maier-Reimer, E., Winguth, A. M., and Archer, D. (1999). A global oceanic sediment model for long-term climate studies. *Global Biogeochemical Cycles*, 13(1):221–250.
- Jeltsch-Thömmes, A., Battaglia, G., Cartapanis, O., Jaccard, S. L., and Joos, F. (2019). Low terrestrial carbon storage at the Last Glacial Maximum: constraints from multi-proxy data. *Climate of the Past*, 15(2):849–879.
- 675 Jeltsch-Thömmes, A. and Joos, F. (2020). Modeling the evolution of pulse-like perturbations in atmospheric carbon and carbon isotopes: The role of weathering–sedimentation imbalances. *Climate of the Past*, 16(2):423–451.

- Jeltsch-Thömmes, A. and Joos, F. (2023). Carbon Cycle Responses to Changes in Weathering and the Long-Term Fate of Stable Carbon Isotopes. *Paleoceanography and paleoclimatology*, 38(2):e2022PA004577.
- 680 Jones, I. W., Munhoven, G., Tranter, M., Huybrechts, P., and Sharp, M. J. (2002). Modelled glacial and non-glacial  $\text{HCO}_3^-$ , Si and Ge fluxes since the LGM: little potential for impact on atmospheric  $\text{CO}_2$  concentrations and a potential proxy of continental chemical erosion, the marine Ge/Si ratio. *Global and Planetary Change*, 33(1-2):139–153.
- Joos, F., Gerber, S., Prentice, I., Otto-Bliesner, B. L., and Valdes, P. J. (2004). Transient simulations of Holocene atmospheric carbon dioxide and terrestrial carbon since the Last Glacial Maximum. *Global Biogeochemical Cycles*, 18(2).
- 685 Joos, F. and Spahni, R. (2008). Rates of change in natural and anthropogenic radiative forcing over the past 20,000 years. *Proceedings of the National Academy of Sciences*, 105(5):1425–1430.
- Jouzel, J., Masson-Delmotte, V., Cattani, O., Dreyfus, G., Falourd, S., Hoffmann, G., Minster, B., Nouet, J., Barnola, J., Chappellaz, J., et al. (2007). EPICA Dome C ice core 800kyr deuterium data and temperature estimates. *IGBP PAGES/World Data Center for Paleoclimatology data contribution series*, 91.
- 690 Kalnay, E., Kanamitsu, M., Kistler, R., Collins, W., Deaven, D., Gandin, L., Iredell, M., Saha, S., White, G., Woollen, J., et al. (1996). The NCEP/NCAR 40-year reanalysis project. *Bulletin of the American meteorological Society*, 77(3):437–472.
- Kemppinen, K., Holden, P. B., Edwards, N. R., Ridgwell, A., and Friend, A. D. (2019). Coupled climate–carbon cycle simulation of the Last Glacial Maximum atmospheric  $\text{CO}_2$  decrease using a large ensemble of modern plausible parameter sets. *Climate of the Past*, 15(3):1039–1062.
- 695 Kerr, J., Rickaby, R., Yu, J., Elderfield, H., and Sadekov, A. Y. (2017). The effect of ocean alkalinity and carbon transfer on deep-sea carbonate ion concentration during the past five glacial cycles. *Earth and Planetary Science Letters*, 471:42–53.
- Kobayashi, H., Oka, A., Yamamoto, A., and Abe-Ouchi, A. (2021). Glacial carbon cycle changes by Southern Ocean processes with sedimentary amplification. *Science Advances*, 7(35):eabg7723.
- Kohfeld, K. E. and Ridgwell, A. (2009). Glacial-interglacial variability in atmospheric  $\text{CO}_2$ . *Surface ocean-lower atmosphere processes*, 187:251–286.
- 700 Köhler, P. and Munhoven, G. (2020). Late Pleistocene carbon cycle revisited by considering solid Earth processes. *Paleoceanography and Paleoclimatology*, 35(12):e2020PA004020.
- Krakauer, N. Y., Randerson, J. T., Primeau, F. W., Gruber, N., and Menemenlis, D. (2006). Carbon isotope evidence for the latitudinal distribution and wind speed dependence of the air–sea gas transfer velocity. *Tellus B: Chemical and Physical Meteorology*, 58(5):390–417.
- 705 Kukla, G., An, Z., Melice, J., Gavin, J., and Xiao, J. (1990). Magnetic susceptibility record of Chinese loess. *Earth and Environmental Science Transactions of the Royal Society of Edinburgh*, 81(4):263–288.
- Lindgren, A., Hugelius, G., and Kuhry, P. (2018). Extensive loss of past permafrost carbon but a net accumulation into present-day soils. *Nature*, 560(7717):219–222.
- 710 Lisiecki, L. E. and Raymo, M. E. (2005). A Pliocene-Pleistocene stack of 57 globally distributed benthic  $\delta^{18}\text{O}$  records. *Paleoceanography*, 20(1).
- Loulergue, L., Schilt, A., Spahni, R., Masson-Delmotte, V., Blunier, T., Lemieux, B., Barnola, J.-M., Raynaud, D., Stocker, T. F., and Chappellaz, J. (2008). Orbital and millennial-scale features of atmospheric  $\text{CH}_4$  over the past 800,000 years. *Nature*, 453(7193):383–386.
- Lüthi, D., Le Floch, M., Bereiter, B., Blunier, T., Barnola, J.-M., Siegenthaler, U., Raynaud, D., Jouzel, J., Fischer, H., Kawamura, K., et al. (2008). High-resolution carbon dioxide concentration record 650,000–800,000 years before present. *nature*, 453(7193):379–382.



- 715 Martin, J. H. (1990). Glacial-interglacial CO<sub>2</sub> change: The iron hypothesis. *Paleoceanography*, 5(1):1–13.
- Menviel, L. and Joos, F. (2012). Toward explaining the Holocene carbon dioxide and carbon isotope records: Results from transient ocean carbon cycle-climate simulations. *Paleoceanography*, 27(1).
- Menviel, L., Joos, F., and Ritz, S. (2012). Simulating atmospheric CO<sub>2</sub>, <sup>13</sup>C and the marine carbon cycle during the Last Glacial–Interglacial cycle: possible role for a deepening of the mean remineralization depth and an increase in the oceanic nutrient inventory. *Quaternary*  
720 *Science Reviews*, 56:46–68.
- Menviel, L., Mouchet, A., Meissner, K. J., Joos, F., and England, M. H. (2015). Impact of oceanic circulation changes on atmospheric  $\delta^{13}\text{CO}_2$ . *Global Biogeochemical Cycles*, 29(11):1944–1961.
- Menviel, L., Timmermann, A., Timm, O. E., and Mouchet, A. (2011). Deconstructing the Last Glacial termination: the role of millennial and orbital-scale forcings. *Quaternary Science Reviews*, 30(9-10):1155–1172.
- 725 Morée, A. L., Schwinger, J., Ninnemann, U. S., Jeltsch-Thömmes, A., Bethke, I., and Heinze, C. (2021). Evaluating the biological pump efficiency of the Last Glacial Maximum ocean using  $\delta^{13}\text{C}$ . *Climate of the Past*, 17(2):753–774.
- Müller, S., Joos, F., Edwards, N., and Stocker, T. (2006). Water mass distribution and ventilation time scales in a cost-efficient, three-dimensional ocean model. *Journal of Climate*, 19(21):5479–5499.
- Müller, S. A., Joos, F., Plattner, G.-K., Edwards, N. R., and Stocker, T. F. (2008). Modeled natural and excess radiocarbon: Sensitivities to  
730 the gas exchange formulation and ocean transport strength. *Global Biogeochemical Cycles*, 22(3).
- Munhoven, G. (2002). Glacial–interglacial changes of continental weathering: estimates of the related CO<sub>2</sub> and HCO<sub>3</sub><sup>-</sup> flux variations and their uncertainties. *Global and Planetary Change*, 33(1-2):155–176.
- Najjar, R., Orr, J., Sabine, C., and Joos, F. (1999). Biotic-HowTo. *Internal OCMIP Report, LSCE/CEA Saclay, Gifsur-Yvette, France*.
- Oliver, K. I., Hoogakker, B. A., Crowhurst, S., Henderson, G., Rickaby, R. E., Edwards, N., and Elderfield, H. (2010). A synthesis of marine  
735 sediment core  $\delta^{13}\text{C}$  data over the last 150 000 years. *Climate of the Past*, 6(5):645–673.
- Opdyke, B. N. and Walker, J. C. (1992). Return of the coral reef hypothesis: Basin to shelf partitioning of CaCO<sub>3</sub> and its effect on atmospheric CO<sub>2</sub>. *Geology*, 20(8):733–736.
- Orr, J. and Epitalon, J.-M. (2015). Improved routines to model the ocean carbonate system: mocsy 2.0. *Geoscientific Model Development*, 8(3):485–499.
- 740 Orr, J., Najjar, R., Sabine, C., and Joos, F. (1999). Abiotic-HowTo. *Internal OCMIP Report, LSCE/CEA Saclay, Gifsur-Yvette, France*, 1999.
- Orr, J. C., Najjar, R. G., Aumont, O., Bopp, L., Bullister, J. L., Danabasoglu, G., Doney, S. C., Dunne, J. P., Dutay, J.-C., Graven, H., et al. (2017). Biogeochemical protocols and diagnostics for the CMIP6 Ocean Model Intercomparison Project (OMIP). *Geoscientific Model Development*, 10(6):2169–2199.
- Parekh, P., Joos, F., and Müller, S. A. (2008). A modeling assessment of the interplay between aeolian iron fluxes and iron-binding ligands  
745 in controlling carbon dioxide fluctuations during Antarctic warm events. *Paleoceanography*, 23(4).
- Peterson, C. D. and Lisiecki, L. E. (2018). Deglacial carbon cycle changes observed in a compilation of 127 benthic  $\delta^{13}\text{C}$  time series (20–6 ka). *Climate of the Past*, 14(8):1229–1252.
- Petit, J.-R., Jouzel, J., Raynaud, D., Barkov, N. I., Barnola, J.-M., Basile, I., Bender, M., Chappellaz, J., Davis, M., Delaygue, G., et al. (1999). Climate and atmospheric history of the past 420,000 years from the Vostok ice core, Antarctica. *Nature*, 399(6735):429–436.
- 750 Pollock, D. E. (1997). The role of diatoms, dissolved silicate and Antarctic glaciation in glacial/interglacial climatic change: a hypothesis. *Global and Planetary Change*, 14(3-4):113–125.

- Pöppelmeier, F., Scheen, J., Jeltsch-Thömmes, A., and Stocker, T. F. (2020). Simulated stability of the AMOC during the Last Glacial Maximum under realistic boundary conditions. *Climate of the Past Discussions*, 2020:1–28.
- 755 Qin, B., Li, T., Xiong, Z., Algeo, T., and Jia, Q. (2018). Deep-Water Carbonate Ion Concentrations in the Western Tropical Pacific Since the Mid-Pleistocene: A Major Perturbation During the Mid-Brunhes. *Journal of Geophysical Research: Oceans*, 123(9):6876–6892.
- Raven, J. A. and Falkowski, P. G. (1999). Oceanic sinks for atmospheric CO<sub>2</sub>. *Plant, Cell & Environment*, 22(6):741–755.
- Ridgwell, A. J., Watson, A. J., Maslin, M. A., and Kaplan, J. O. (2003). Implications of coral reef buildup for the controls on atmospheric CO<sub>2</sub> since the Last Glacial Maximum. *Paleoceanography*, 18(4).
- 760 Roberts, J., Gottschalk, J., Skinner, L. C., Peck, V. L., Kender, S., Elderfield, H., Waelbroeck, C., Vázquez Riveiros, N., and Hodell, D. A. (2016). Evolution of South Atlantic density and chemical stratification across the last deglaciation. *Proceedings of the National Academy of Sciences*, 113(3):514–519.
- Roth, R., Ritz, S., and Joos, F. (2014). Burial-nutrient feedbacks amplify the sensitivity of atmospheric carbon dioxide to changes in organic matter remineralisation. *Earth System Dynamics*, 5(2):321–343.
- 765 Sarnthein, M., Schneider, B., and Grootes, P. M. (2013). Peak glacial <sup>14</sup>C ventilation ages suggest major draw-down of carbon into the abyssal ocean. *Climate of the Past*, 9(6):2595–2614.
- Schmitt, J., Schneider, R., Elsig, J., Leuenberger, D., Lourantou, A., Chappellaz, J., Köhler, P., Joos, F., Stocker, T. F., Leuenberger, M., et al. (2012). Carbon isotope constraints on the deglacial CO<sub>2</sub> rise from ice cores. *Science*, 336(6082):711–714.
- Schmittner, A. (2003). Southern Ocean sea ice and radiocarbon ages of glacial bottom waters. *Earth and Planetary Science Letters*, 213(1-2):53–62.
- 770 Schmittner, Andreas Galbraith, E. D. (2008). Glacial greenhouse-gas fluctuations controlled by ocean circulation changes. *Nature*, 546.
- Schneider, R., Schmitt, J., Köhler, P., Joos, F., and Fischer, H. (2013). A reconstruction of atmospheric carbon dioxide and its stable carbon isotopic composition from the penultimate glacial maximum to the last glacial inception. *Climate of the Past*, 9(6):2507–2523.
- Shackleton, N. J. (2000). The 100,000-year ice-age cycle identified and found to lag temperature, carbon dioxide, and orbital eccentricity. *Science*, 289(5486):1897–1902.
- 775 Siegenthaler, U., Stocker, T. F., Monnin, E., Luthi, D., Schwander, J., Stauffer, B., Raynaud, D., Barnola, J.-M., Fischer, H., Masson-Delmotte, V., et al. (2005). Stable carbon cycle climate relationship during the Late Pleistocene. *Science*, 310(5752):1313–1317.
- Sigman, D. M. and Boyle, E. A. (2000). Glacial/interglacial variations in atmospheric carbon dioxide. *Nature*, 407(6806):859–869.
- Sigman, D. M., Hain, M. P., and Haug, G. H. (2010). The polar ocean and glacial cycles in atmospheric CO<sub>2</sub> concentration. *Nature*, 466(7302):47–55.
- 780 Smith, H. J., Fischer, H., Wahlen, M., Mastroianni, D., and Deck, B. (1999). Dual modes of the carbon cycle since the Last Glacial Maximum. *Nature*, 400(6741):248–250.
- Stein, K., Timmermann, A., Kwon, E. Y., and Friedrich, T. (2020). Timing and magnitude of Southern Ocean sea ice/carbon cycle feedbacks. *Proceedings of the National Academy of Sciences*, 117(9):4498–4504.
- Stephens, B. B. and Keeling, R. F. (2000). The influence of Antarctic sea ice on glacial–interglacial CO<sub>2</sub> variations. *Nature*, 404(6774):171–
- 785 174.
- Tschumi, T., Joos, F., Gehlen, M., and Heinze, C. (2011). Deep ocean ventilation, carbon isotopes, marine sedimentation and the deglacial CO<sub>2</sub> rise. *Climate of the Past*, 7(3):771–800.
- Tschumi, T., Joos, F., and Parekh, P. (2008). How important are Southern Hemisphere wind changes for low glacial carbon dioxide? A model study. *Paleoceanography*, 23(4).

- 790 Von Blanckenburg, F., Bouchez, J., Ibarra, D. E., and Maher, K. (2015). Stable runoff and weathering fluxes into the oceans over Quaternary climate cycles. *Nature Geoscience*, 8(7):538–542.
- Wallmann, K., Schneider, B., and Sarnthein, M. (2016). Effects of eustatic sea-level change, ocean dynamics, and nutrient utilization on atmospheric pCO<sub>2</sub> and seawater composition over the last 130 000 years: a model study. *Climate of the Past*, 12(2):339–375.
- Wanninkhof, R. (2014). Relationship between wind speed and gas exchange over the ocean revisited. *Limnology and Oceanography: Methods*, 12(6):351–362.
- 795 Weiss, R. (1974). Carbon dioxide in water and seawater: the solubility of a non-ideal gas. *Marine chemistry*, 2(3):203–215.
- Willeit, M., Ganopolski, A., Calov, R., and Brovkin, V. (2019). Mid-Pleistocene transition in glacial cycles explained by declining CO<sub>2</sub> and regolith removal. *Science Advances*, 5(4):eaav7337.
- Winckler, G., Anderson, R. F., Fleisher, M. Q., McGee, D., and Mahowald, N. (2008). Covariant glacial-interglacial dust fluxes in the equatorial Pacific and Antarctica. *science*, 320(5872):93–96.
- 800 Wood, M., Hayes, C. T., and Paytan, A. (2023). Global Quaternary Carbonate Burial: Proxy-and Model-Based Reconstructions and Persisting Uncertainties. *Annual review of marine science*, 15:277–302.
- Yu, J., Menviel, L., Jin, Z., Thornalley, D., Foster, G. L., Rohling, E., McCave, I., McManus, J., Dai, Y., Ren, H., et al. (2019). More efficient North Atlantic carbon pump during the last glacial maximum. *Nature communications*, 10(1):2170.
- 805 Yu, Z., Loisel, J., Brosseau, D. P., Beilman, D. W., and Hunt, S. J. (2010). Global peatland dynamics since the last glacial maximum. *Geophysical research letters*, 37(13).